METROLOGICAL EVALUATION OF SIZE SPECIFICATIONS IN ISO 14405-1

by

Yue Peng

A thesis submitted to the faculty of
The University of North Carolina at Charlotte
in partial fulfillment of the requirements
for the degree of Master of Science in
Mechanical Engineering

Charlotte

2015

Approved by:

_____
Dr. Edward P. Morse

_____
Dr. Gert Goch

_____
Dr. Jimmie Miller

ABSTRACT

YUE PENG. Metrological evaluation of size specifications in ISO 14405-1. (Under the direction of DR. EDWARD P. MORSE)

The international standard ISO 14405-1 was released in 2010 as part of the geometrical product specifications (GPS) of the ISO system. This document provides standardized definitions of linear sizes. Most notably, it has expanded the linear size specifications from the ISO default specification operator — the two-point size — to 14 types of sizes. This richer scope of size specifications is intended to assist the geometric dimensioning and tolerancing (GD&T) of products.

To clarify the semantics of the size specifications and to understand their application in conformance assessment, this thesis evaluated 8 of the sizes, offering computational algorithms, experimental data processing, numerical results and interpretations of results. Two types of features, a cylinder and a constant width shaped part are covered as physical examples for the evaluations of the sizes. The latter feature provides insights into the conformance of some traditional measurement methods of two-point size to the standard, for example measurements with vernier calipers. Geometric evaluations of these features were carried out on data sets collected with coordinate measuring machines (CMMs). The sources of uncertainty in the calculations of some sizes were analyzed, including uncertainty introduced by individual measured points and influence of sampling density.

ACKNOWLEDGMENTS

I would like to extend my sincerest appreciation to my advisor, Dr. Edward P. Morse, who offered professional, diligent and encouraging guidance for this research project. With his generous offer of the research opportunity, supervision, effective advises and constant help, I got a chance to gain insight into metrology, GD&T, as well as rigorous and professional research methods. Great gratitude goes to Mr. Greg Caskey for help with obtaining the data and offering insightful advises in the analyses.

Many thanks to Dr. Gert Goch and Dr. Jimmie Miller for serving on the committee of this thesis. Thank you so much for your valuable supports and advises. Thanks to National Institute of Standards and Technology for the financial support granted through the project.

Finally gratitude to my family, colleagues and friends, for your kind support, encouragements and valuable comments.

TABLE OF CONTENTS

LIST OF TABLES

LIST OF FIGURES

CHAPTER 1: INTRODUCTION

Size is one of the qualities of a mechanical product specified by the designer according to its physical functions. It ensures the specific description of a product together with form, location and orientation [1] [2]. Especially required in assemblies and for the interchangeability of the products, dimensions and tolerances are assigned to each component to be controlled, so that it will fit as designed. Standards have been set up to offer guidance of how to specify these size specifications with defined symbols and operators [3] [4].

Traditionally, size definitions and the geometric dimensioning and tolerancing (GD&T) are in accordance with conformance gages and two-point measurement devices. Therefore, the default size specifications have been the global fitting size and two-point size. With the demand for tighter tolerances and more various functional requirements of the products, and with the development of more flexible and efficient measurement methods such as coordinate metrology, more sophisticated and specific size descriptions are needed.

ISO published 14405-1 [5] in 2010 to offer definitions of linear size specifications. 14 types of sizes are defined. Before their applications in metrology practices, the semantics of these specifications has to be fully understood, as well as how to assess the conformance of actual features to the nominal based on these specifications. Especially with coordinate information collected from coordinate measuring machines (CMMs),

how to associate or calculate the actual size needs to be looked into. Investigations are also needed to identify the sensitiveness of these calculated actual values, to the deviations of the part, to the measurement errors in the coordinates of sampled points, and to the mathematical calculation procedure. With proper interpretation of the standard, another important question is whether these specifications are actually useful and effective in GD&T practices. These questions raised by the new standard form the motivations and objectives of this project and this thesis.

As for the scope of this thesis, 8 of the sizes are evaluated, including two-point size, least-squares size, and 6 rank-order sizes. Of the modifiers, two-point size and least-squares size have been commonly applied in metrology practices. The rank order sizes are statistical characteristics based on a set of local sizes. The evaluations are carried out for the sizes of two features: a cylinder and a constant width shaped part.

The constant width shaped part offers insights into how the shape of the part impacts its conformance evaluation with the specifications. The constant width shape consists of 6 arcs, which are centered about three different centers and each has either a radius of a larger size R or a smaller size r (FIGURE 1.1). The three centers form an equilateral triangle whose side length is a. By constant width, it means the width of the shape, or the distance between two parallel planes containing the shape, measures constantly regardless of the direction of the tangents.

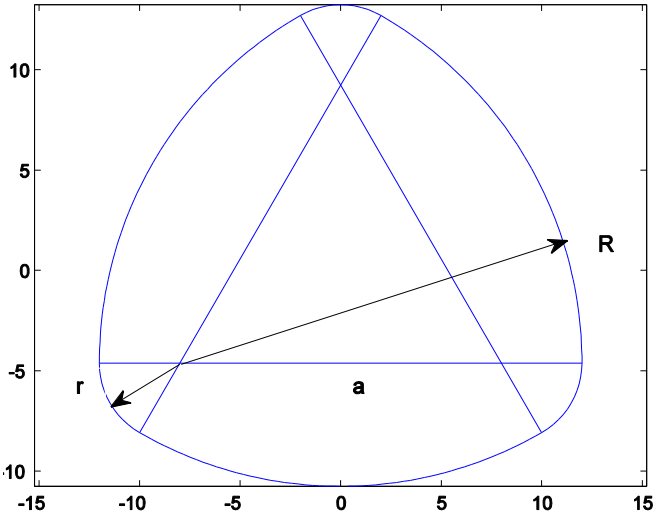

FIGURE 1.1: Schematics of a constant width shape

A literature review is offered in Chapter 2 including the discussions about size as a notion, popular methods for applying least-squares criterion and issues related to two-point size. Chapter 3 offers the experimental preparations, including the features measured, the simulated and measured data.

Least-squares criterion is a widely understood association method. The algorithms of least-squares association are offered for the two features in Chapter 4. Coordinate metrology offers high efficiency sampling of the two measured parts. Sampling density affects how much information is extracted from the measured feature; therefore its influence on the association result is to be investigated. Measuring errors exist in each measured point. How the uncertainties in individual points contribute to the uncertainty of the size association is under discussion.

Two-point size is physically analogous to the measurements of hand gages and two-point measurement devices, for example the micrometers and calipers in traditional metrology. This criterion requires the conformance of the actual feature at different

sampling locations. The sampling strategy will impact the conformance assessment since the extreme points might not be sampled. Coordinate metrology offer more flexible sampling strategies with larger sample density, but would involve mathematical calculation from coordinates to distance between two points. The algorithms are discussed in Chapter 5, as well as their impacts on the final result.

The rank-order sizes are statistically based on the ordering of the local sizes, two-point sizes specifically for this thesis. They are influenced by the result of two-point sizes. Rank-order sizes for the two features are calculated and presented in Chapter 6.

Chapter 7 offered comments on the study and suggestions for further study.

CHAPTER 2: LITERATURE REVIEW

2.1. Size

The meaning of ‘size’ as a notion has been revisited by metrologists since the 1990s. H. B. Voelcker explored the meaning of ‘size’ in a series of publications [6, 7, 8], offering discussions into the conceptions of size and possible solutions of conformance assessments. E. P. Morse [1] followed the development of size tolerancing strategies, conformance assessment and evolutions in standards in 2013. It has been a continuous effort to review the understanding of size, and renovate the specifications to meet the design demands.

With GD&T specified, the conformance of the actual size of a feature to the nominal size is examined and assessed. The conventional size tolerances consist of an upper limit and a lower limit [1]. Traditionally, the actual feature is examined with conformance gauges and two-point measurements devices. For example, to assess the outer diameter of a cylinder, conformance gauges examine the upper size limit and the calipers examine the lower limit. Based on the conventional measurement practices, the default size specifications have been the global fitting size and two-point size.

While the traditional gauges are still withholding their significance in metrology, the development of coordinate metrology benefits geometric measurements with better sampling capability and efficiency. Coordinate metrology enables the possibilities of more flexible conformance assessments, thus possibilities of more various size

specifications of features. This raise questions in size specifications, that how to assess the conformance now with the coordinates of sampled points, whether the default specifications are able to fulfill and exactly describe the various design intentions, and how to develop the size specifications to take the advantages of coordinate metrology. ISO made an approach to offer more size specifications, hoping to assist the product design and GD&T.

2.2. ISO 14405-1

ISO 14405- 1 [5], published in 2010, is the first part of the geometrical product specifications (GPS) of dimensional tolerance by ISO, which offers definitions of specification operators for linear sizes. Sizes are defined through features of size in the ISO system. ISO 5459:2011 [9] defines 5 features of size: cylinder, sphere, parallel planes, cone and wedge. The former 3 are the bases for defining linear sizes, the latter for angular sizes. ISO 14405-2:2011 [10] offers specifications for sizes other than linear sizes.

The specification operators in 14405-1 are referred to as modifiers. The modifiers are applied to dimensions on an engineering drawing, constraining and clarifying the dimensions to be controlled. TABLE 2.1 shows a list of the linear sizes defined in ISO 14405-1, the symbols, descriptions and classifications are displayed.

TABLE 2.1: Specification modifiers for linear size

Modifier	Description	Type of specification
(LP)	Two-point size	Local size
(LS)	Local size defined by a sphere	Local size
(GG)	Least-squares association criterion	Global size
(GX)	Maximum inscribed association criterion	Global size
(GN)	Minimum circumscribed association criterion	Global size

TABLE 2.1: Continued

CC	Circumference diameter	Calculated size
CA	Area diameter	Calculated size
CV	Volume diameter	Calculated size
SX	Maximum size	Rank-order size
SN	Minimum size	Rank-order size
SA	Average size	Rank-order size
SM	Median size	Rank-order size
SD	Mid-range size	Rank-order size
SR	Range of sizes	Rank-order size

There are three groups of sizes: local size, global size, and calculated size. Local size is defined at a single local point or one pair of points, "having by definition a non-unique result of evaluation along and/or around the feature of size" [5]. Whereas, the global size is implemented on the entire feature, a section of the feature, or a population of local sizes, which is "having by definition a unique result of evaluation along and around the tolerance feature of size" [5]. The global size includes the rank-order sizes. The calculated size is "obtained by using a mathematical formula that relates the intrinsic characteristic of a feature to one or several other dimensions of the same feature" [5].

2.3. Least-squares Criterion

The least-squares criterion is a widely implemented association criterion. V. Srinvasan et al [11] investigated the reasons for the wide implementation and enduring appeal of least-squares fitting.

To establish the associated feature or size from actual measured points according to least-squares criterion, the fitted feature is determined by minimizing the sum of squares of the deviations between the data points and the fitted feature. If the deviations in the data points with regard to the fitted feature are denoted by $e_i, \mathrm{i} = 1,2, \ldots, \mathrm{n}$ for n points, the best fit of the data points are obtained when

$$\sum_{i=1}^{n}(e_i)^2 \rightarrow \min \qquad (2.1)$$

e_i could be defined according to the shape of feature.

Different algorithms for solving the least-squares problem have long been developed, for example Gauss-Newton method, and Levenberg-Marquardt method are two of the most well-known ones for non-linear least-squares problem [12]. Nelder–Mead method is also a popular method in non-linear optimization [13]. National organizations publish documents on least-squares algorithms as references. For example National Institute of Standards and Technology (NIST) of USA published their algorithms and an algorithm testing system [14], and National Physical Laboratory (NPL) of UK also published their algorithms for finding the least-squares best-fit geometric elements to data [15]

2.4. Two-point Size

The conventional two-point measurement devices find the two-point size by containing the part in two opposing parallel faces as tangent planes, which should contact the feature at theoretically two points. These two contacting points would certainly be the two outmost points at the measured line, or in other words, the measured distance is the largest distance the two parallel measuring faces could touch. For rotation-invariant features such as a circle, a cylinder, a sphere and for two opposing parallel planes, these contacting points form a pair of opposite points. Therefore the measured distance is the two-point size, as defined in ISO 14405-1, being the distance between two ‘opposite’ points.

However, for certain features, the two points seen by the measuring surfaces of a caliper or micrometer are not necessarily a pair of opposite points(180 degrees apart,

relative to the center of the shape). The constant width shape under discussion in this thesis is an example that this assumption is not valid (FIGURE 2.1). The measuring surfaces see the "measured distance" in the figure, but the two-point distance is through the center of the feature, which is not accessible with these devices. With the sampled points from coordinate metrology, however, the two-point distance could be obtained by mathematical searching for opposite points and then interpolation.

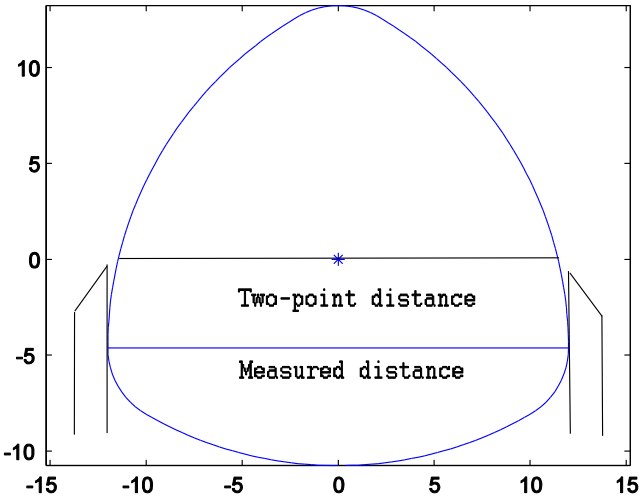

FIGURE 2.1: Measured distance and two-point distance for constant width part

CHAPTER 3: EXPERIMENTAL PREPARATIONS

Two physical features were measured as instances in this thesis: a cylinder and a constant width shaped part. Cylinder is one of the features of size in ISO [9], and all specifications are evaluated as diameter specifications, which are the least-squares diameter, two-point diameter and rank-order diameters. The least-squares result of the constant width shaped part is a set of parameters that constructs the shape. The two-point size and rank-order sizes of the constant width shaped part has some specific characteristics to be discussed due to its shape.

Both measured data and simulated data were used in the experiments for calculation. In the simulated data, the parameters for constructing the feature and the additional errors could be controlled. 'Perfect parts' was generated to verify the functionality of the algorithms. Various error sources were introduced and adjusted to test the robustness of the algorithms and to investigate the sensitivity of the calculation to errors. Measured data offered more complex variations of the data in the actual situations, which was largely related to the manufacturing processes.

3.1. Measured Data

Two physical parts were measured with continuous contact scanning on a Zeiss Prismo CMM with the VAST Gold probe head [15].

Two different diameters on one cylinder, as shown in FIGURE 3.1, were measured with a 3mm diameter stylus and 30 mm extension. The upper cylinder with a

diameter of approximately 101.61 mm, referred to as ‘Part A’ in this paper, was measured with 10 levels of cross-sections, approximately 1.3 mm separation from each other, and 490 points on each level. The bottom cylinder with a diameter of approximately 104.05 mm is referred to as ‘Part B’ in this paper, and was measured with 10 levels of cross-sections, approximately 1.5 mm separation from each other, and 492 points on each level. The overshooting points in the scanning procedure were removed, and the stylus radius was corrected by the measuring machine.

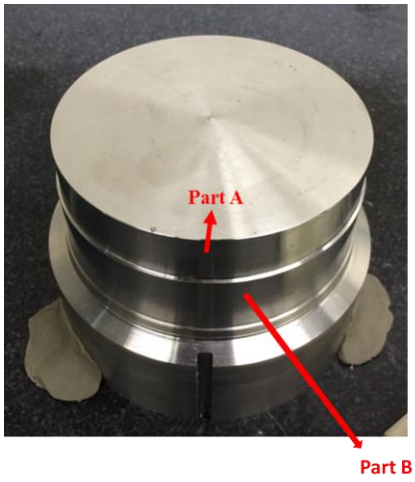

FIGURE 3.1: Cylinder containing Part A and Part B

The third feature measured was a prismatic part with constant width shape as cross-sections, referred to as ‘Part C’ in the following discussion (FIGURE 3.2). Part C was measured with 5 mm probe, with the curve scanning function of the machine. It has a constant width of approximately 23.95 mm, and was measured with 20 levels of 168 points, each level 1 mm from another. The stylus radius was corrected by the measuring machine.

FIGURE 3.2: Measured Part C

3.2. Simulated Data

Simulated cylinders are constructed based on 5 parameters (x, y, l, m, R) (FIGURE 3.3). (x, y) defines the center of the reference surface, (l, m) defines the orientation of the axis, and R is the radius of the cylinder. The samples are generated with even increments of center angle for each cross section and even increments in the axial direction for different levels. A text document containing the (X, Y, Z, I, J, K) information of the designed points are generated for the simulated cylinder, and is read into the least-squares fitting program later as input points.

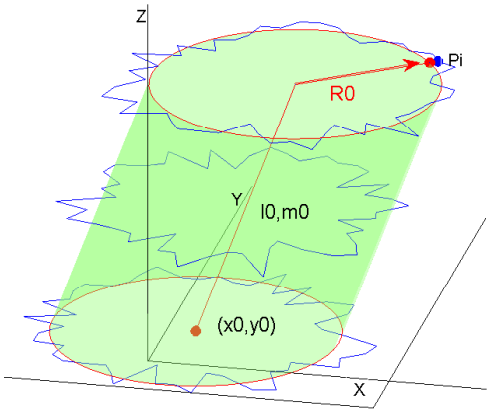

FIGURE 3.3: Model of a cylinder [16]

The first simulated cylinder is a reference part, which is a prefect cylinder with no deviation, referred to as Part CYL_S1 in the following discussion. The design parameters are:

$$(x_0, y_0, l_0, m_0, R_0) = (0,0,0,0, 50)$$

with units of (x_0, y_0, R) being mm and units of (l_0, m_0) being radian. Other features of the cylinder include

$h = 100\ mm$, the height of the cylinder, level height ranging from 0 to 90 mm with 10 mm increments;

$nh = 10$, number of levels of cross-sections;

$nth = 500$, number of points per cross-section;

$n = 10 * 500 = 5000$, total number of points;

The second simulated cylinder, referred to as Part CYL_S2 is designed with deviations or errors in the parameters:

$$(x_0, y_0, l_0, m_0, R) = (0.1, 0.1, 0.001, 0.001, 50)$$

with units of (x_0, y_0, R) being mm and units of (l_0, m_0) being radian. The rest of the features are the same with CYL_S1.

Additionally, normally distributed random errors are added to the radius of each point to simulate the form variations on a real part, the standard deviation of the distribution being $dev = 20\ \mu m$.

Simulated constant width shaped parts are constructed based on 7 parameters $(x, y, m, l, a, b, \theta)$ (FIGURE 3.4). a is side length of the equilateral triangle formed by the centers, b is the extension to the sides as the smaller radius, (x, y, m, l) defines the center and axis of the prismatic shape, and θ defines the rotation about z axis since this is a

rotational variant part. The samples are generated with even increments of arc length in each cross section, which is in accordance with the scanning measurement of the actual part. In the axial direction, the sampled levels are in even increments.

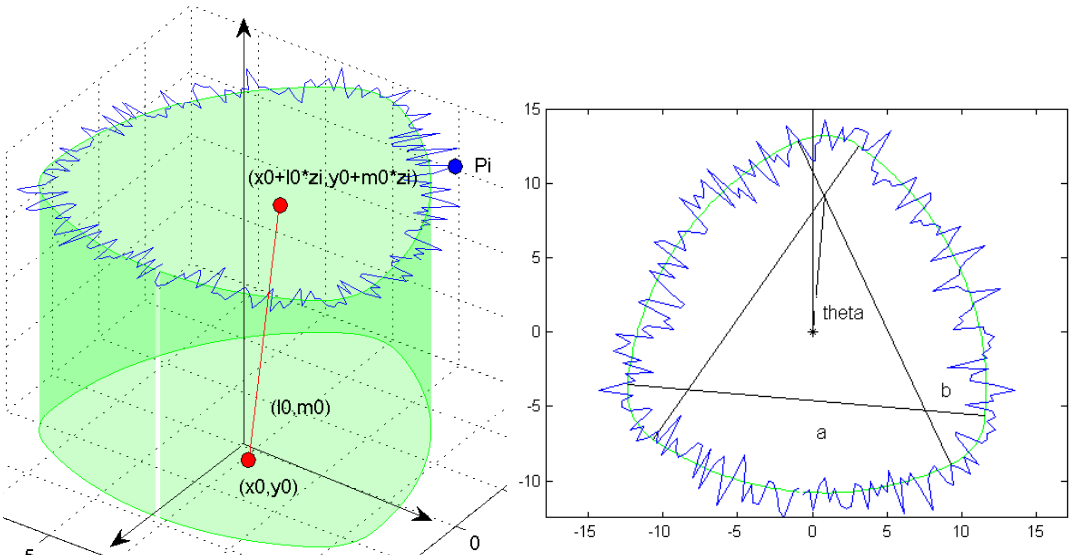

FIGURE 3.4: Model of constant width part

The first simulated part is a reference part, referred to as Part CWP_S1. The designed primary parameters are:

$$(x_0, y_0, l_0, m_0, a, b, \theta) = (0,0,0,0,16,4,0)$$

with unit of (x_0, y_0, a, b) being mm and unit of (l_0, m_0) being radian. This part is simulated to be 20 mm in height, levels increments to be 1 mm. 20 levels and 216 points on each cross-section are simulated. Total number of points $n = 20 * 216 = 4320$. No form error was added to this simulation, which means this is a perfect part.

The second simulated part is simulated with deviations, referred to as Part CWP_S2. The design parameters are:

$$(x_0, y_0, l_0, m_0, a, b, \theta) = (0.01, 0.01, 0.001, 0.001, 16,4,0.0873)$$

with unit of (x_0, y_0, a, b) being mm and unit of (l_0, m_0, θ) being radian. Normally distributed random errors were added to the radius of each point, the standard deviation of the distribution being $dev = 10\ \mu m$. The rest of the features are same with CWP_S1.

CHAPTER 4: LEAST-SQUARES SIZE

According to the least-squares criterion, the fitted feature is determined by minimizing the sum of squares of the deviations between the data points and the fitted feature. For the cylinder, e_i is defined as deviation in the radius from the actual point to the fitted feature, which is the difference between the radial distance of each point to the fitted center and the fitted radius. The detailed algorithms are explained in Section 4.1. For the constant width part, e_i is also defined as deviation in the radial direction, but the radial distance of each point is relative to the fitted center of the specific arc it belongs to, instead of the center of the entire feature.

The algorithm for solving the least-squares optimization in this thesis is based on the Gaussian-Newton method for non-linear least-squares solution of the cylinder [17] and a built-in function in Matlab, which is based on the Nelder–Mead "simplex" algorithm for the constant width shaped part [13].

4.1. Algorithms of Least-squares Size

4.1.1. Algorithms for the Least-squares Diameter of a Cylinder

A cylinder surface, based on the five parameters $\boldsymbol{X} = (x_0, y_0, l_0, m_0, R_0)^T$, could be modeled as FIGURE 4.1. (x_0, y_0) is the translation of the center point on the reference surface from the origin of the alignment. (l_0, m_0) is the tilt of the cylinder axis. R_0 is the fitted radius of the cylinder. The deviation of an arbitrary point Pi to the fitted cylinder surface could be given as Equation (4.1) [17], if the axis is aligned with z axis.

$$e_i = r_i - (R_0 + x_0 \cos\theta_i + y_0 \sin\theta_i + l_0 z_i \cos\theta_i + m_0 z_i \sin\theta_i) \qquad (4.1)$$

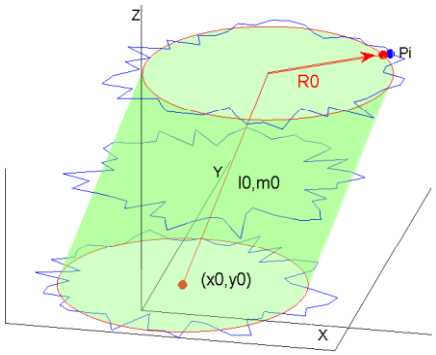

FIGURE 4.1: Deviation model of a cylinder, translation and tilt

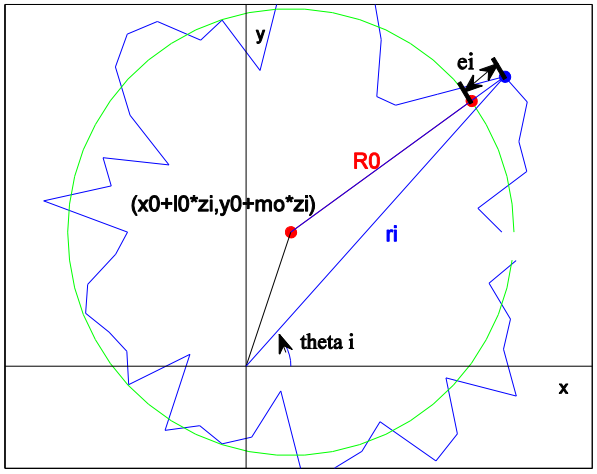

FIGURE 4.2: Deviation model of a cylinder, an arbitrary cross section

Since the part is non-linear deviated away from the origin, the points are adjusted or transformed first to be well aligned with the coordinate system, then the model could be used in the fitting. While the part is properly aligned with the coordinate system, this is a linear problem. However for the initial alignments, this is a non-linear least squares optimization, and the Gauss–Newton algorithm is implemented to find the minimum of the square sum of the residuals. The objective function is

$$\mathbf{S} = \sum_{\boldsymbol{i=1}}^{\boldsymbol{N}} \boldsymbol{e_i^2}, \qquad (4.2)$$

$\mathrm{N} = 1,2, \ldots$ is the total number of points.

$\boldsymbol{A}_i$ is a vector of coefficients for $\boldsymbol{X}$, which is made up of (r_i, z_i, θ_i) of the point index i.

$$\boldsymbol{A_i} = [\cos\theta_i\,,\ \sin\theta_i\,, z_i\cos\theta_i\,, z_i\sin\theta_i\,, 1]; \qquad (4.3)$$

$$e_i = r_i - \boldsymbol{A}_i \cdot \boldsymbol{X} = r_i - \sum_{j=1}^{5} A_{i,j} \cdot X_j \ \ ; \qquad (4.4)$$

$$\boldsymbol{r} = [r_i, r_2, \ldots, r_N]^T; \qquad (4.5)$$

$\mathrm{j} = 1,2, \ldots, 5,$ is the index of the parameters.

To find the least-squares optimization, set the partial derivatives for each parameter to zero, so the equation for the j th parameter would be

$$\frac{\partial S}{\partial X_{\boldsymbol{j}}} = \sum_{i=1}^{N} 2 \cdot e_i \cdot \frac{\partial e_i}{\partial \boldsymbol{X_j}} = 0; \qquad (4.6)$$

$$\sum_{i=1}^{N}\left[\left(r_i - \sum_{k=1}^{5} A_{i,k} \cdot X_k\ \right) \cdot \frac{\partial\left(r_i - \sum_{k=1}^{5} A_{i,k} \cdot X_k\ \right)}{\partial X_{\boldsymbol{j}}}\right] = 0;$$

$$\sum_{i=1}^{N}\left[\left(r_i - \sum_{k=1}^{5} A_{i,k} \cdot X_k\ \right) \cdot \left(-A_{ij}\right)\right] = 0;$$

$$\sum_{i=1}^{N}\left(r_i \cdot A_{ij}\right) - \sum_{i=1}^{N}\left[A_{ij} \cdot \left(\sum_{k=1}^{5} A_{i,k} \cdot X_k\ \right)\right] = 0;$$

$$\sum_{i=1}^{N}\left(r_i \cdot A_{ij}\right) = \sum_{i=1}^{N}\sum_{k=1}^{5} A_{i,j} \cdot A_{i,k} \cdot X_k\,, \qquad \mathrm{j} = 1,2, \ldots, 5;$$

$$\boldsymbol{A}_j^T \cdot \boldsymbol{r} = \boldsymbol{A}_j^T \cdot \boldsymbol{A} \cdot \boldsymbol{X}; \qquad (4.7)$$

$\boldsymbol{A_j}$ *is the jth colomn of* $\boldsymbol{A}$

Put the equations for all the parameters in a group,

$$\boldsymbol{A^T \cdot r = A^T \cdot A \cdot X;} \qquad (4.8)$$

Solve the equation for $\boldsymbol{X}$,

$$\boldsymbol{X = \ (A^T \cdot A)^{-1} \cdot A^T \cdot r;} \qquad (4.9)$$

The iteration process is shown in FIGURE 4.3.

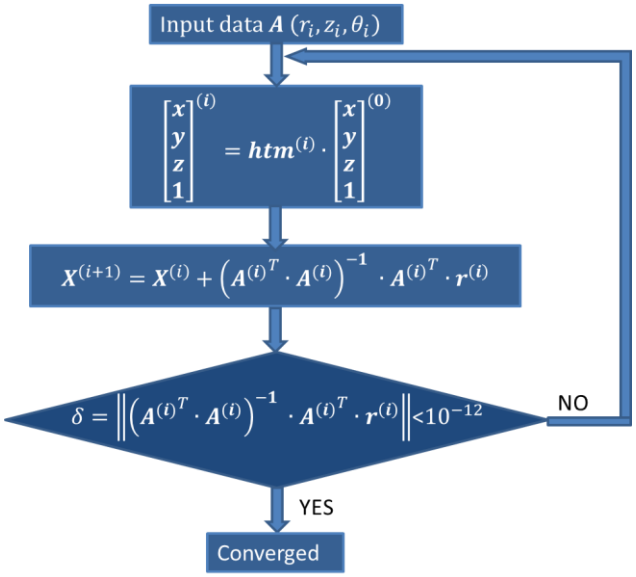

FIGURE 4.3: Flow chart of least-squares diameter calculation

Firstly, an initial guess $\boldsymbol{X^{(0)}}$ is offered for the first iteration. With the (x_0, y_0, l_0, m_0) from the guess, the original points are translated so that the center is on z axis, and then rotated so the axis is aligned with z axis. For the following iterations, since a better alignment is achieved by solving the former iteration, an adjusted guess $\boldsymbol{X^{(i)}}((i)$ marking the cycle of iteration) offers the transformation. Transformations are carried out by imposing a matrix $\boldsymbol{htm}$ generated from $\boldsymbol{X^{(0)}}$ or $\boldsymbol{X^{(i)}}$.

$$\boldsymbol{htm}^{(i)} = \boldsymbol{R}_y^{(i)} \cdot \boldsymbol{R}_x^{(i)} \cdot \boldsymbol{T}^{(i)}$$

$$= \begin{bmatrix} \cos\left(-\tan^{-1} l_0^{(i)}\right) & 0 & \sin\left(-\tan^{-1} l_0^{(i)}\right) & 0 \\ 0 & 1 & 0 & 0 \\ -\sin\left(-\tan^{-1} l_0^{(i)}\right) & 0 & \cos\left(-\tan^{-1} l_0^{(i)}\right) & 0 \\ 0 & 0 & 0 & 1 \end{bmatrix}$$

$$\cdot \begin{bmatrix} 1 & 0 & 0 & 0 \\ 0 & \cos\left(\tan^{-1} m_0^{(i)}\right) & -\sin\left(\tan^{-1} m_0^{(i)}\right) & 0 \\ 0 & \sin\left(\tan^{-1} m_0^{(i)}\right) & \cos\left(\tan^{-1} m_0^{(i)}\right) & 0 \\ 0 & 0 & 0 & 1 \end{bmatrix}$$

$$\cdot \begin{bmatrix} 1 & 0 & 0 & -x_0^{(i)} \\ 0 & 1 & 0 & -y_0^{(i)} \\ 0 & 0 & 1 & 0 \\ 0 & 0 & 0 & 1 \end{bmatrix}; \qquad (4.10)$$

$$\begin{bmatrix} \boldsymbol{x} \\ \boldsymbol{y} \\ \boldsymbol{z} \\ \boldsymbol{1} \end{bmatrix}^{(i)} = \boldsymbol{htm}^{(i)} \cdot \begin{bmatrix} \boldsymbol{x} \\ \boldsymbol{y} \\ \boldsymbol{z} \\ \boldsymbol{1} \end{bmatrix}^{(0)} \qquad (4.11);$$

$\boldsymbol{R}_y$ and $\boldsymbol{R}_x$are rotational matrix about the y axis and x axis. $\boldsymbol{T}$ is the translation matrix to z axis. The translation is carried out first, and then the rotations.

As the result of one iteration, after solving the final matrix function for $\boldsymbol{X}$, the increments in the parameters to get a better alignment or closer fitting is gained. The guess for the next iteration would be

$$\boldsymbol{X}^{(i+1)} = \boldsymbol{X}^{(i)} + \left(\boldsymbol{A}^{(i)^T} \cdot \boldsymbol{A}^{(i)}\right)^{-1} \cdot \boldsymbol{A}^{(i)^T} \cdot \boldsymbol{r}^{(i)}, \qquad i = 0,1,2, \ldots, \qquad (4.12)$$

The residuals of the points are

$$\boldsymbol{res} = \boldsymbol{A}^{(i)} \cdot \left(\boldsymbol{A}^{(i)^T} \cdot \boldsymbol{A}^{(i)}\right)^{-1} \cdot \boldsymbol{A}^{(i)^T} \cdot \boldsymbol{r}^{(i)} - \boldsymbol{r}^{(i)}; \qquad (4.13)$$

The difference of one guess from its former guess is

$$\delta = \left\| \left(\boldsymbol{A}^{(i)^T} \cdot \boldsymbol{A}^{(i)}\right)^{-1} \cdot \boldsymbol{A}^{(i)^T} \cdot \boldsymbol{r}^{(i)} \right\|; \qquad (4.14)$$

The iteration stops when the difference of the two guesses is within an acceptable amount, which is set to 10^{-12}. This difference is set equal to 1 for the initial guess so it enters the loop for the first time.

4.1.2. Algorithm of the Least-squares Fitting of a Constant Width Part

A constant width part could be modeled with 7 parameters: $(x_0, y_0, l_0, m_0, a, b, \theta)$. (x_0, y_0) are the translation of the center point from the origin of the alignment on the reference surface. (l_0, m_0) are the tilt of the axis. a is the side length of the equilateral triangle formed by centers of the arcs, b is the smaller radius of the two radii, $\mathrm{b} = \mathrm{r}$, as shown in FIGURE 4.4. The larger radius would be $\mathrm{R} = \mathrm{a} + \mathrm{b}$. θ is the rotation about the axis, because the constant width shape is rotational variant.

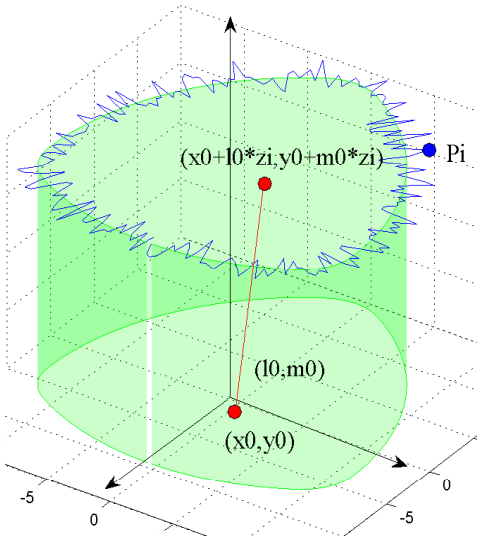

FIGURE 4.4: Deviation model of a constant width part, translation and tilt of axis

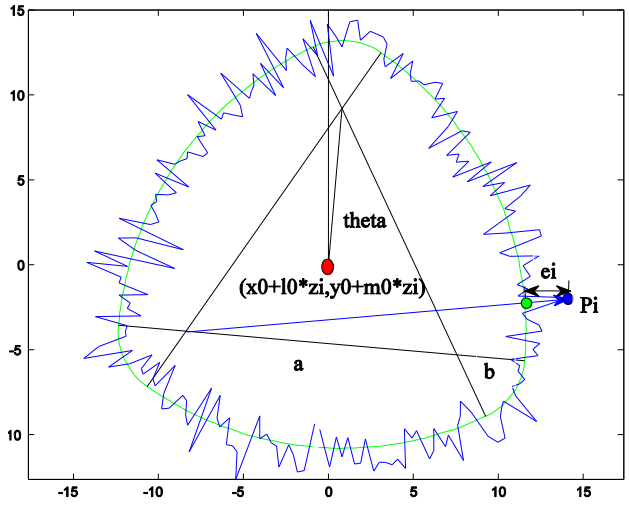

FIGURE 4.5: Deviation model of a constant width part, an arbitrary cross section

The deviation of an arbitrary point P_i to the fitted surface could be given as e_i as shown in FIGURE 4.5. e_i equals the difference between the distance of P_i to the center of the arc that P_i belongs to (distance denoted by d_i), and the radius of that arc. Then the least-squares fitting procedure is to find the minimum of the square sum of the deviation of each point.

$$S = \sum_{i=1}^{N} e_i^2, \qquad (4.15)$$

$N = 1,2, \ldots$ is the total number of points.

The iteration process is shown in FIGURE 4.6.

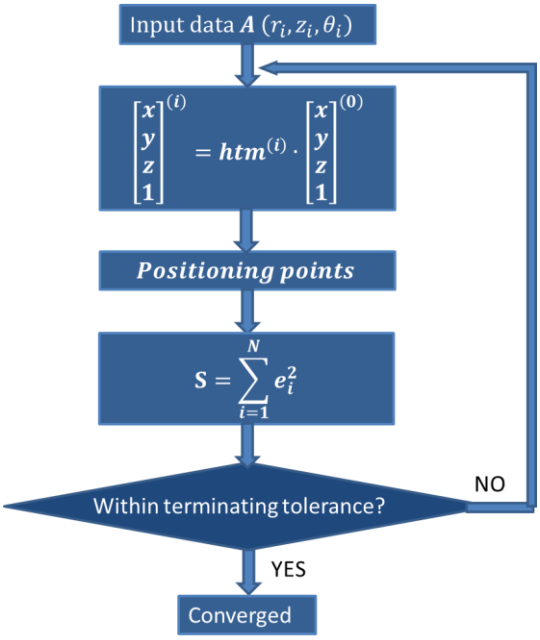

FIGURE 4.6: Flow chart of least-squares fitting of the constant width part

Firstly, the points are transformed, same with the first step for the cylinders. Secondly, since the points belong to different arcs, each point needs to be located before calculating the deviation. When the part is well aligned, the three centers of the arcs could be offered based on the geometry of the constant width shape (FIGURE 4.7), which are $\left(0,\ \frac{\sqrt{3}}{3}a\right)$, $\left(-\frac{1}{2}a, -\frac{\sqrt{3}}{6}a\right)$, and $(\frac{1}{2}a, -\frac{\sqrt{3}}{6}a)$. The central angle of an arbitrary point P_i about each center is calculated. The position of point P_i is decided by matching these three central angles with the angle range of the arcs (Table 4.1).

TABLE 4.1: Positioning of points

Center	Angle Range	Corresponding Arc	d_i	e_i
$\left(0, \frac{\sqrt{3}}{3}a\right)$	$\left[-\frac{2}{3}\pi, -\frac{\pi}{3}\right)$	Arc1	P_i to $\left(0,\ \frac{\sqrt{3}}{3}a\right)$	$e_i = d_i - R$
$\left(-\frac{1}{2}a, -\frac{\sqrt{3}}{6}a\right)$	$\left(-\pi, -\frac{2}{3}\pi\right)$ & π	Arc2	P_i to $\left(-\frac{1}{2}a, -\frac{\sqrt{3}}{6}a\right)$	$e_i = d_i - r$

TABLE 4.1: Continued

$\left(\frac{1}{2}a, -\frac{\sqrt{3}}{6}a\right)$	$\left[\frac{2}{3}\pi, \pi\right)$	Arc3	P_i to $\left(\frac{1}{2}a, -\frac{\sqrt{3}}{6}a\right)$	$e_i = d_i - R$
$\left(0, \frac{\sqrt{3}}{3}a\right)$	$\left[\frac{\pi}{3}, \frac{2}{3}\pi\right)$	Arc4	P_i to $\left(0, \frac{\sqrt{3}}{3}a\right)$	$e_i = d_i - r$
$\left(-\frac{1}{2}a, -\frac{\sqrt{3}}{6}a\right)$	$[0, \frac{\pi}{3})$	Arc5	P_i to $\left(-\frac{1}{2}a, -\frac{\sqrt{3}}{6}a\right)$	$e_i = d_i - R$
$\left(\frac{1}{2}a, -\frac{\sqrt{3}}{6}a\right)$	$\left[-\frac{\pi}{3}, 0\right)$	Arc6	P_i to $\left(\frac{1}{2}a, -\frac{\sqrt{3}}{6}a\right)$	$e_i = d_i - r$

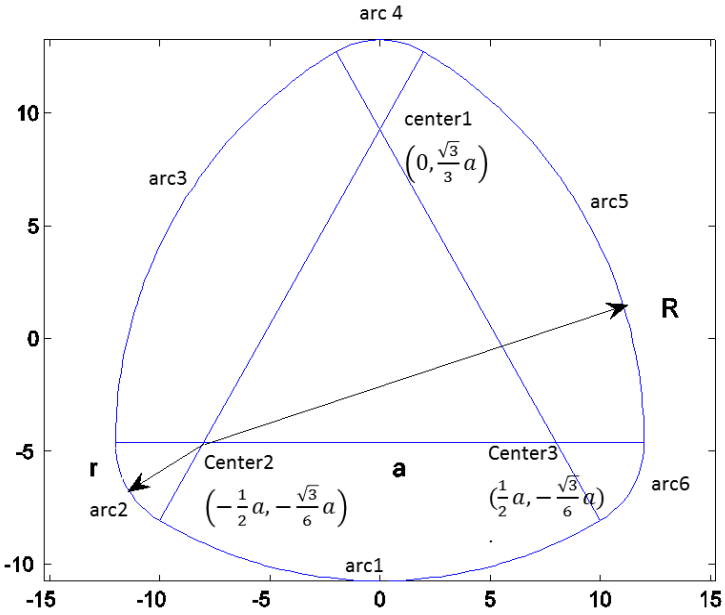

FIGURE 4.7: A well-aligned constant width shape

Finally, the approximation is done with the objective function being $S = \sum_{i=1}^{N} e_i^2$ by the Nelder-Mead simplex algorithm [13]. The algorithm first makes a simplex around the initial guess, and modifies the simplex repeatedly by processes such as reflecting, expanding, and contracting. A function in Matlab, **`fminsearch`**, could be used to find the minimum of S, as well as the best fit parameters to reach the minimum.

4.2. Application to Simulated and Measured Data

For each part, including the simulated and measured part, an initial guess was offered and a fitted feature was calculated. The residual deviations could be an indicator of how far the individual points are from the fitted cylinder. The least-squares residual $Res = \sum_i^n res_i^2, i = 1,2, \dots, n$, is thus offered in the following analyses for reference.

4.2.1. Least-squares Diameter of Simulated and Measured Cylinders

For Part CYL_S1, with initial guess $(x_0, y_0, l_0, m_0) = (0, 0, 0, 0)$, the fitted cylinder was $(x, y, l, m, R) = (-8.36 \cdot 10^{-15}, -8.12 \cdot 10^{-15}, 1.07 \cdot 10^{-15}, 9.78 \cdot 10^{-17}, 49.999999999966440)$. $Res = 3.5 \cdot 10^{-14} mm^2$ for 5000 points. This fitting of 'perfect' data shows a level of numerical errors remaining due to the resolution of the computer calculation and the stopping criterion of the fitting algorithm.

For Part CYL_S2, with initial guess $(x_0, y_0, l_0, m_0) = (0, 0, 0, 0)$, the fitted cylinder was $(x, y, l, m, R) = (\ 0.0988, 0.0995, 0.0010, 0.0010, 50.0004)$. $Res =$ 1.98 $mm^2$for 5000 points.

The upper measured cylinder, or Part A, with initial guess $(x_0, y_0, l_0, m_0) = (0, 0, 0, 0)$, the fitted cylinder was $(x, y, l, m, R) = (\ -0.0622,\ 0.0132, -0.0001, -0.0007,\ 50.8036)$. $Res = 0.0071\ mm^2$for 4900 points.

One cross section of the fitted cylinder with exaggerated deviation is shown in FIGURE 4.8. The deviations are magnified by 5000 times. Besides the form deviations of the surface shown with blue lines, Part A exhibits some systematic deviations from a perfect circle at each cross-section, as shown by the difference of the fitted circle (red line) and the average circle (dashed black line). The diameter in the horizontal direction of this

figure is apparently shorter than that in the vertical direction. As a result, the two-point size (calculated in Chapter 5) shows a periodic waving pattern. The cross-section shown in FIGURE 4.8 is the one of the cross-sections, but this systematic deviation is typical for all cross-sections.

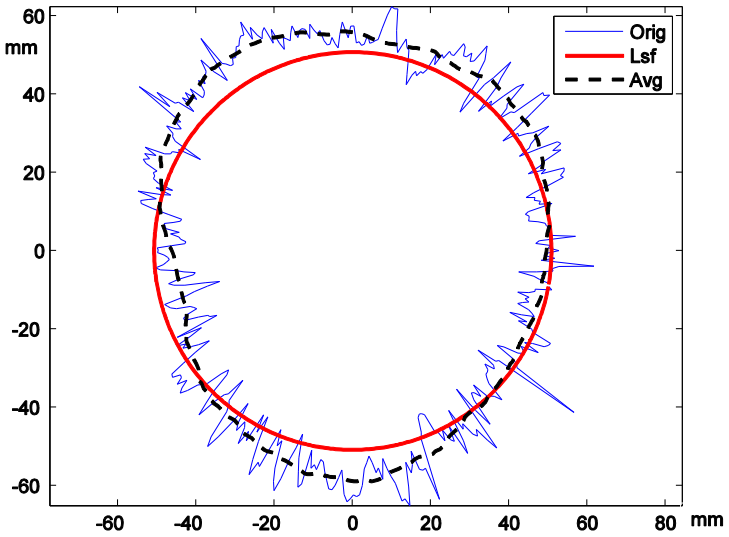

FIGURE 4.8: A cross section of fitted Part A, magnification of deviation: 5000

For the bottom measured cylinder, or Part B, with initial guess $(x_0, y_0, l_0, m_0) = (0, 0, 0, 0)$, the fitted cylinder was $(x, y, l, m, R) = (-0.0008, -0.0007, -0.0000, -0.0000, 52.0224)$. $Res = 0.005\ mm^2$ for 4920 points. Similar to Part A, the bottom cylinder also bears some systematic deviations from a circle in each cross-section, but it is less deviated than part A. However, there are more "spikes" on part B, due to the form characteristics of the surface or possibly dirt.

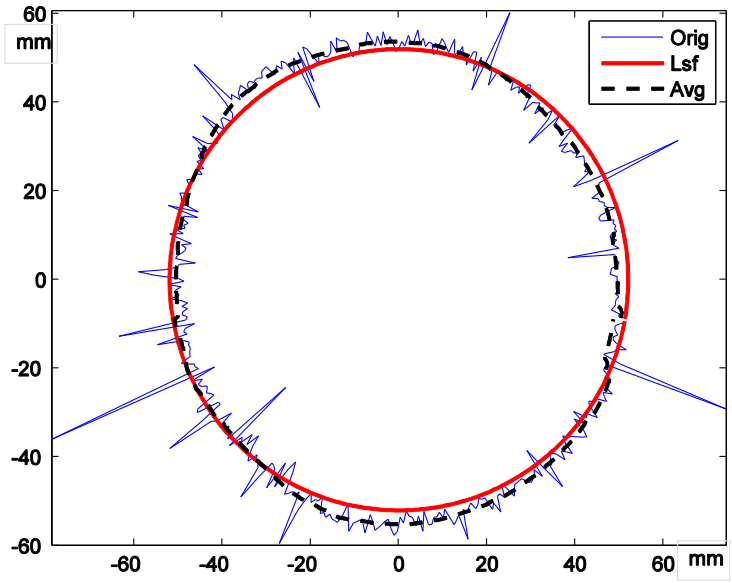

FIGURE 4.9: A cross section of fitted Part B, magnification of deviation: 5000

If average the residual to each point, by dividing the residual by the number of points and taking the square root, the average residual in each point is approximately 1.2 μm for Part A and 1.0 μm for Part B, which indicates how close the fitting is.

4.2.2. Verification with NIST Reference Data and Results for Cylinders

NIST offers a sequence of data sets and their least-squares fits as references for industrial self-checking. The data sets of NIST were fed into the program of this thesis as input points, and the fitted results were compared with those offered by NIST. The result format of NIST is different from our set up, which is given by 7 numbers, 3 representing a point on the cylinder axis, 3 representing the direction cosines of the axis, and 1 representing the diameter of the cylinder. To verify our program with NIST references, the results need to be formatted.

There are some limitations of the program used in this thesis when tested with the reference data sets.

Firstly, our program is based on a model that the cylinder reference surface is aligned with the x-y plane. While in practice, the measured cylinder will also be basically aligned, so the z coordinates are not adjusted. The (x_0, y_0) in the model is the intersection of the axis with the $z = 0$ plane. Therefore, if the cylinder is far above or below the z origin, or it is in very large angle with z axis and far from the origin of the coordinate system, the initial guess of the center coordinates are very large or possibly tends to be infinity. As a result, the matrices in the fitting procedure might not behave well, thus not yielding a proper result. In this case, the original data could be transformed first to be better aligned with z axis for the convenience of calculation.

Secondly, the initial guess plays an important role. Improper initial guess may lead to non-converging iterations. Better initial guesses offer a closer start for the iteration, and may converge to a closer result of estimation, leaving smaller residuals. The effect of the initial guess is not significantly shown in the calculation of the cylinders because the deviation model is relatively simple and is a linear model. When it comes to irregular shapes, for example the constant width part, the effect of initial guess will be more obvious, as could be seen in section 4.2.3.

As an example of the verification, the fitted diameter from NIST of the first set of cylinder data is 57.289229507551100877, and from our program is 57.289229507551056. Therefore, our result agrees to the 12^{th} digits in this case.

4.2.3. Least-squares Fitting of Simulated and Measured Constant Width Part

The effect of initial guess is much more obvious on the least-squares fitting result of this part than the cylinder.

For least-squares fitting of Part CWP_S1, Table 4.2 is a list of initial guesses, with the corresponding resulted convergence detector, fitted parameters, the residual of the objective function, and the calculation time of Matlab.

TABLE 4.2: Experiments about initial guess with Part CW_S1

Initial guess	Convergence	Fitted result	Residual (Res, mm^2)	Cal. Time (s)
$(0,0,0,0,0,0,0)$	No			
$(0,0,0,0,10,0,0)$	Yes	$(0.0189, -0.0222, -0.0094, 0.0246, 23.607$ $-0.0133, -0.0151)$	$1.886 \cdot 10^{3}$	30
$(0,0,0,0,10,5,0)$	Yes	$(-0.0016, -0.0001, 0.0001, 0.0000, 16.0000,$ $-0.0000)$	$7.176 \cdot 10^{-4}$	18
$(0,0,0,0,15,5,0)$	Yes	$(0.0004, -0.0001, -0.0000, 0.0000, 16.0000,$ $-0.0000)$	$5.860 \cdot 10^{-5}$	17
$(0,0,0,0,16,4,0)$	Yes	$(0,0,0,0,16,4,0)$	$3.455 \cdot 10^{-14}$	4

With initial guess $(x_0, y_0, l_0, m_0, a, b, \theta) = (0,0,0,0,0,0,0)$, the result was not converging. The missing of dimension information (a, b) made it difficult to find the proper solution. As the initial guess gets closer to the designed value, the fitted result gets closer to the designed value, the residual gets smaller and the calculation time gets shorter.

For Part CWP_S2, with initial guess $(x_0, y_0, l_0, m_0, a, b, \theta) = (0,0,0,0,0,0,0)$ the result was also not converging. With initial guess $(x_0, y_0, l_0, m_0, a, b, \theta) = (0,0,0,0,16,4,0)$ the fitted parameters were $(x_0, y_0, l_0, m_0, a, b, \theta) = (-0.0107,\ -0.0080,\ 0.0010,\ 0.0010,\ 15.9990,\ 4.0004,\ 0.0872)$. The best initial guess should be the designed parameters. With initial guess $(x_0, y_0, l_0, m_0, a, b, \theta) = (0.01,\ 0.01,\ 0.001,\ 0.001, 16,\ 4,\ 0.0873)$ the fitted

parameters were $(x_0, y_0, l_0, m_0, a, b, \theta) = (-0.0104,\ -0.0091,\ 0.0009,\ 0.0010,\ 15.9993,\ 4.0003,\ 0.0872)$. The residual was 0.087 mm^2 for 4320 points, and the calculation time was 17s.

For the measured Part C, the estimations of $(a, b) = (16, 4)$ are expected, according to approximated hand measurements. With initial guess $(x_0, y_0, l_0, m_0, a, b, \theta) = (0,0,0,0,0,0,0)$ the result was not converging. With initial guess $(x_0, y_0, l_0, m_0, a, b, \theta) = (0,0,0,0,16,4,0)$ the fitting result was $(x_0, y_0, l_0, m_0, a, b, \theta) = (-0.0032,\ -0.0012,\ -0.0006,\ -0.0006,\ 15.9439, 3.9871,\ 0.0074)$. Since the nominal parameters were not available, better convergence could only be reached by using the fitted result as initial guess and running the calculation again. After optimizing the initial guess for 3 times, the fitted result tended to reach the best fit. The initial guess was $(x_0, y_0, l_0, m_0, a, b, \theta) = (-0.0154,\ -0.0117,\ 0.0002,\ 0.0001,\ 15.9454,\ 3.9863,\ 0.0073)$, and the fitted result was $(x_0, y_0, l_0, m_0, a, b, \theta) = (-0.0151,\ -0.0112,\ 0.0002,\ 0.0001,\ 15.9455,\ 3.9863,\ 0.0073)$. The residual was 4.4131 mm^2 for 3360 points, and the calculation time was 7.44s.

The average residual in each point for Part C was approximately 36.1μm, which was not as tight a fitting as the cylinders. This is partially due to the complex shape of the part, the limitation of finding the best initial guess, and the actual characteristics of the measured part, which has defects shown in FIGURE 4.10.

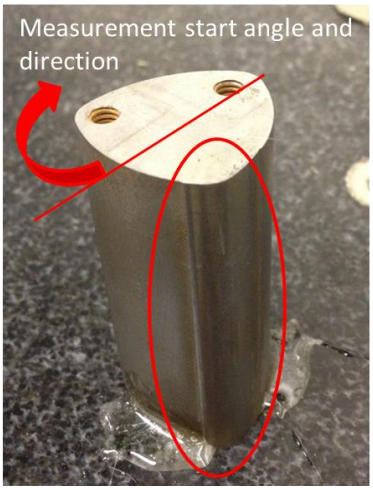

FIGURE 4.10: Defect on Part C

4.3. Uncertainty in the Calculation of Least-squares Diameter of Cylinder

The errors come from 4 major sources in a practical CMM measurement and least-squares calculation procedure:

1. Measurement errors, mainly coming from the machine errors, including the probing error (since we scanned the parts, this error would be the scanning error of the probe head), angular errors of all the machine axes, and squareness errors of the machine axes.

2. Errors caused by the least-squares fitting procedure. The fitting procedure is an optimization procedure, and the convergence of the iterations is set to a limited extend, so errors will be introduced.

3. Errors introduced by sampling. CMM obtain sampled points form the part, so the sampling strategy and density introduce errors into the calculation.

4. Errors introduced by environment variations, for example temperature variation, or unstable fixtures.

A comprehensive uncertainty analysis should be a task specific analysis including all possible error sources. Since many items listed above were not accessible during the time period of this project, and it was the effects of the least-squares procedure that is concerned in this thesis, only the second part of all the errors are discussed in details here, and the third part is discussed in section 4.3.2. This is not intended to be a comprehensive analysis, and the purpose is to show how sensitive is the least-squares size to factors such as the errors in the input points and sampling. As one instance of the analysis, data of part A is used in the following analysis.

4.3.1. Uncertainty Analysis of Least-squares Fitting of a Cylinder

This is a non-linear least-squares optimization, so a Monte Carlo process [19] is used in the uncertainty analysis. Least-squares fitting of the constant width part take at least several seconds, making the Monte Carlo process time consuming. Therefore, uncertainty analysis of least-squares fitting of a cylinder is offered as an example in the following section.

As inputs into the optimization procedure, coordinates of each point contain errors as covered in the first group of error sources above. At the time of this analysis, good estimations for the angular and squareness errors of the machine were not provided. An experiment with simulated error terms was done by artificially feeding 1-5 arcsec each error term respectively into the data of part A, and checking the deviation caused in the least-squares result. This test was only valid for the purpose of checking the influence of angular and squareness errors of the machine, not valid for a rigorous uncertainty analysis. The result showed that the change in the fitted radius after feeding in most of the error terms was less than 0.5 nm. However, for some terms, the fitted radius was changed for

more than 1 nm, which was comparable to the amount of uncertainty offered by the following analysis.

The scanning error was introduced based on the specification of the machine with type B evaluation. It was associated to each point and propagated into the iteration procedure of fitting by the Monte Carlo process. The machine was a Zeiss PRISMO 7 with ultra sensors and ultra accuracy, and the probe was VAST Gold. According to the specification sheet [16], the MPE (maximum permissible error) of the scanning error is$1.1\mu m$. According to ISO 10360-4:2000 [20], the scanning error could be modeled as range of change in radial distance (r_i) of each point. It is uniformly distributed, within the interval of $[-0.55\mu m, 0.55\mu m]$.

The Monte Carlo propagation procedure is shown in FIGURE 4.11.

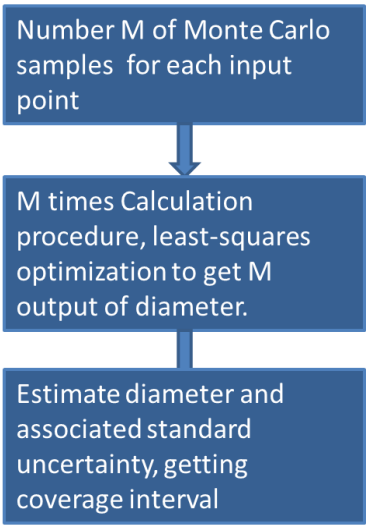

FIGURE 4.11: Procedure of uncertainty analysis with Monte Carlo method

M variations were introduced into each measured point, forming M groups of input points. M times of calculations were conducted and M least-squares diameters were

calculated. M=100,000 in the following offered result, and the entire procedure was done in Matlab, within 636 seconds.

The probability histogram is shown in FIGURE 4.12. The best estimation is the mean of all resulted R

$$\bar{R} = 50.8036419\, mm$$

Combined uncertainty is the uncertainty of mean

$$u_c = 1.4 \times 10^{-6}\text{mm}$$

Therefore, the least-squares radius is offered as

$$\bar{R} = 50.8036419 \pm 1.4 \times 10^{-6} mm$$

with coverage factor k=1.

The least-squares diameter is offered as

$$\bar{D} = 101.6072838 \pm 2.7 \times 10^{-6} mm$$

with coverage factor k=1.

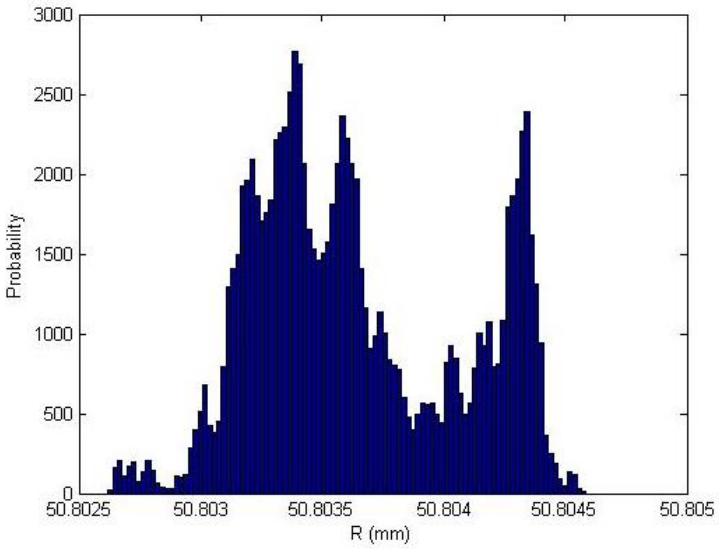

FIGURE 4.12: Probability histogram: the result radii from the Monte Carlo procedure

From this rough analysis, if the uncertainty introduced by the input points is in sub micro meter level, the uncertainty after the least-squares procedure would be nanometer level. This uncertainty should be interpreted as the uncertainty of the 'average' effect of the least-squares procedure.

4.3.2. Influence of Sampling

To obtain subsets of data with different point density, smaller samples are extracted directly from the original measured data set. The first group of data set is the original data, which contains all the measured points. The second group of data sets is obtained by taking every second point of the measured points, so there are two sets of data in the second group, the odd numbered points and the even numbered points, and each contains half of the number of points of the original points. The third group of data sets is obtained by taking every third point of the measured points, so there are three sets of data in the third group, and each contains one third of the number of points of the original points.

Each set of points is evaluated independently. For each set of points, the least-squares diameter was calculated, and results of all the data sets of all the groups (50 groups in total) were plotted. The following figures show the least-squares size distribution with respect to the number of points used in the evaluation. FIGURE 4.13 shows the least-squares diameter of Part CYL_S2. FIGURE 4.14 shows that of part A and FIGURE 4.15 shows that of part B.

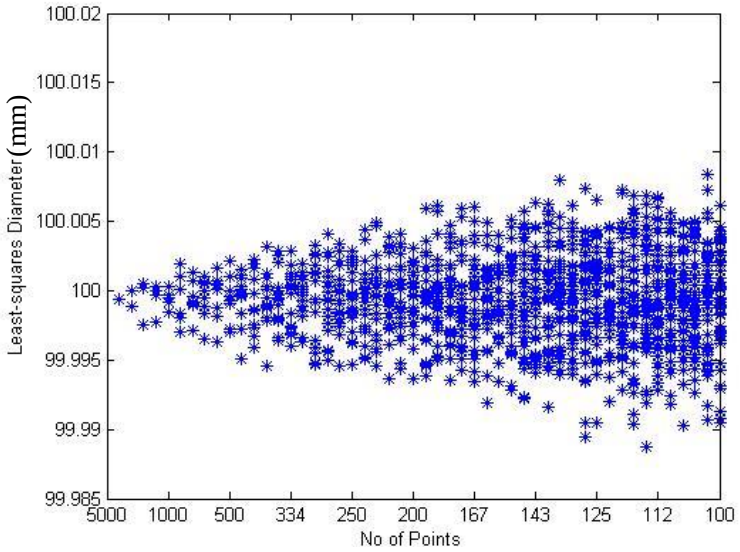

FIGURE 4.13: Least-squares diameters of subsets of simulated data

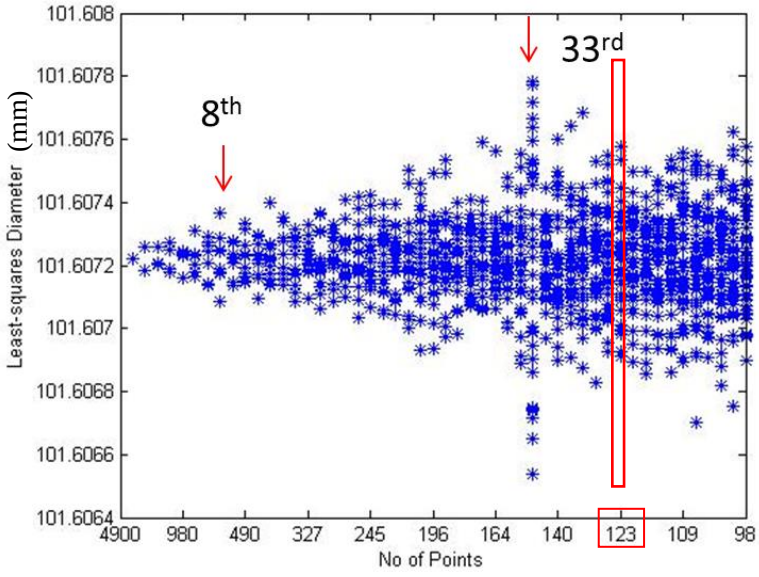

FIGURE 4.14: Least-squares diameters of subsets of measured part A

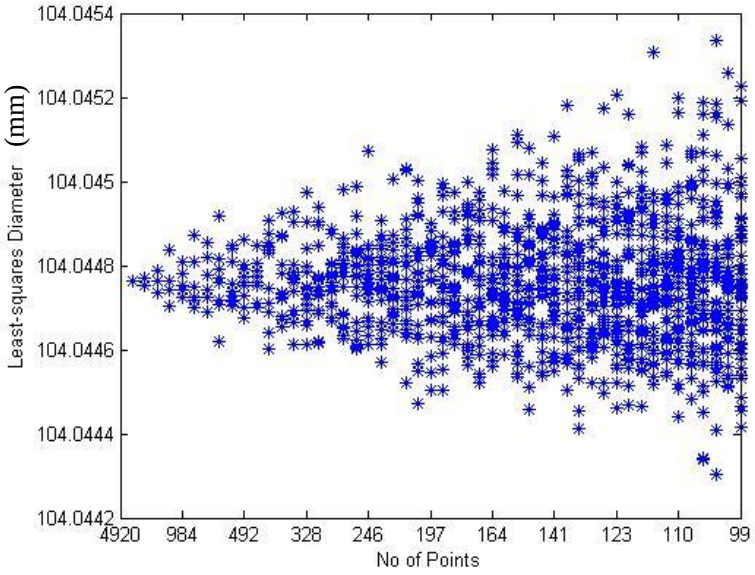

FIGURE 4.15: Least-squares diameters of subsets of measured part B

The least-squares diameter shows more dispersion with fewer sampled points, which means a larger uncertainty due to the sampling density introduced into the least-squares result. A type A evaluation of the uncertainty could be done for each group of diameters [21]. Take the group with 123 sampling points in the Part A groups as an example, as shown in FIGURE 4.14. There are 40 sets of data in this group, therefore 40 diameter values. There's a possibility to arrive at any one of the values within the dispersion of this group if 123 sampling points are taken to calculate the least-squares diameter. With a type A evaluation, the best estimation, which is the mean of the 40 values, is 101.607221, and the uncertainty of the mean is 24 nm.

The result of the bottom cylinder (FIGURE 4.15) shows similar trend as simulated data. However, the result of Part A shows some more characteristics. The dispersion of the results for the 33rd group of data sets, the subsets in which contain 148 or 149 points, is much larger than the other groups, as marked in FIGURE 4.14. A

possible reason is the interaction of the sampled points with the cutter marks on the part surface.

To verify this assumption, the frequency property of the radius values of all the points after the alignment was investigated. Characteristics of the radius values show the characteristics of the part surface. FIGURE 4.16 was obtained by carrying out the Fourier transform of the radius values, and the Frequency axis represents the spatial frequency of the surface moving along the circumference. The dominating frequency was at 0, in correspondence with the constant value of radius. All the other frequencies are at 10 to the -5 to 10 to the -4 order of magnitude. If eliminating the dominating frequency, a closer examine of the rest of the frequency components is shown in FIGURE 4.16.

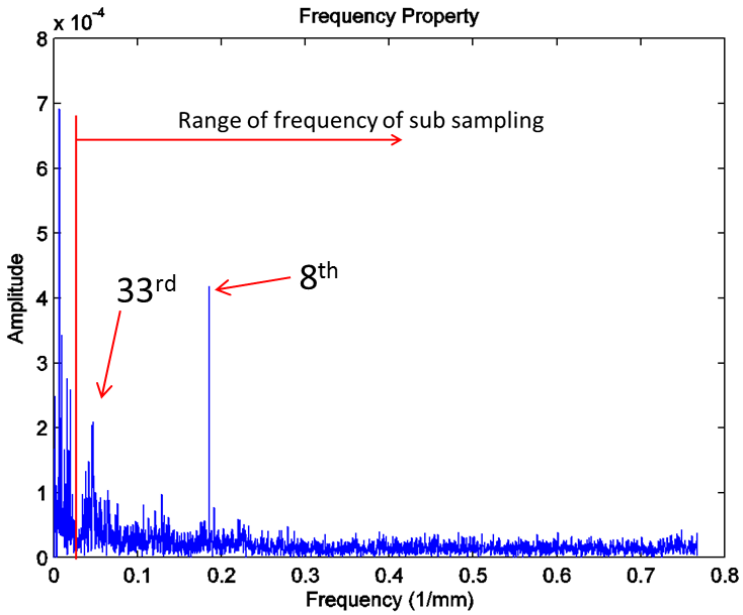

FIGURE 4.16: Frequency components of radius values of part A

To focus on the frequency range that are in accordance with the sampling frequencies of the sub sets, and present the frequency axis in the form of group index of the sub sets, an adjusted figure is offered as FIGURE 4.17. X axis is the sampling factor

because the index of the sub sample group is also the factor of reducing the sample density. There are 3 outstanding peaks corresponding to the 8th and 33th group of sampling. Referring back to the diameter distribution of the subsets, the 33th group shows much larger dispersion than other groups. The dispersion of group 8 is relatively larger than group 7 and 9, but due to the limitation of only 8 data points, the increase in the dispersion is not significant.

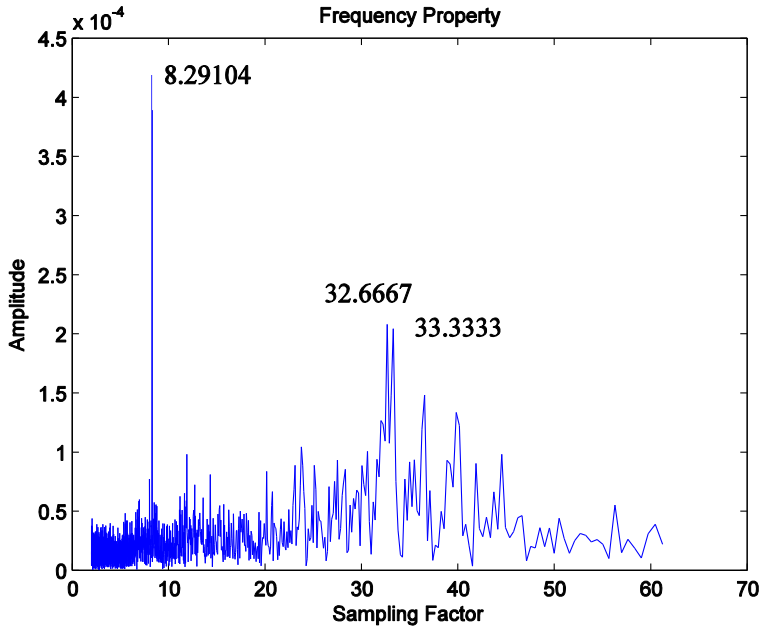

FIGURE 4.17: Frequency components of radius values of part A

The initial sampling frequency of the measured points is $\mathrm{Fs} = \frac{n}{10 \cdot 2\pi R}$ points per mm. n is the total number of sampling points, 10 is the number of levels, $2\pi R$ is the arc length per level, and R could be estimated with the least-square radius. For Part A, $\mathrm{Fs} = 1.5350471643/\mathrm{mm}$. The spatial frequency corresponding to group 8 is 1/8 of the initial sampling frequency, which is $\mathrm{F}_8 = 0.1918808955$, and that of group 33 is $\mathrm{F}_{33} = \frac{1}{33}\mathrm{Fs} = 0.0465165807$. These peaks could be identified in FIGURE 4.16 as well.

Therefore, there are some characteristics of the part surface interacting with the sampling. These characteristics might come from the manufacturing process.

CHAPTER 5: TWO-POINT SIZE

5.1. Introduction into Two-point Size

The two-point size is one of the default operators for size in the ISO system. It is a local size and is defined as “distance between two opposite points taken on the feature of size” in ISO 14405-1 [5]. Tolerancing with two-point size theoretically requires that the infinite number of points on the feature be in conformance with the tolerance. In the measurement practice, the measurement is usually done on multiple points at different locations on the feature.

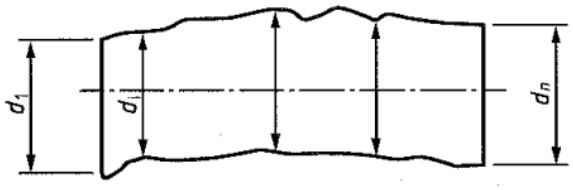

FIGURE 5.1: Two-point definition from ISO 14405-1:2010

As explained in Chapter 2, for some features the two-point size at certain points might not be accessible with gages. With coordinate measuring devices, sample points at these locations could be obtained and the two-point sizes could be calculated. Since it is not secured that both the point and its opposite point are sampled in the measurement process, the key point in calculation becomes how to locate the corresponding opposite point with information of its adjacent sampled points.

ISO 14660-2 requires that the extracted surface be perpendicular to the associated cylinder axis, and the connection line between the local size points includes the

associated circle center [22]. These requirements are only indicated on cylinders as a feature of size. CWP is not a standard feature of size, these requirements could be interpreted as that the extracted surface should be perpendicular to the associated feature axis, and the connection line between the local points includes the associated center of cross-section.

In the actual measurements, the measured data was sampled in the same height in the machine coordinate system, which means the sampled points might not be exactly on the plane perpendicular to the associated cylinder axis. The evaluations of two-point size were carried out still with the original sampled points but the distances were calculated in the cross-sections perpendicular to the axis (FIGURE 5.2) and added up to form the two-point distance. Therefore the two "opposite points" are actually not in the same plane. For example, according to the fitted axis information offered in Section 4.2.1, the slope of the axis of part A is 1/(-0.0007) in x-z plane, the misalignment of the two points $\Delta = \frac{D}{tan\delta} \approx D \cdot (-0.0007) \approx -70\ \mu m$ along the axis of the part. Although there is a misalignment, the evaluated distance in FIGURE 5.1 is still a good approximation of the two-point size since they are evaluated perpendicular to the axis and the radial change over 70μm along the axis is very small.

Since the two opposite points are actually not on the same perpendicular plane to the axis, the associated center of the cross section needs to be approximated by the associated axis. In a word, the two-point size is calculated by adding up the radial distances of the two points, and the radial distances are the distances from the point perpendicular to the associated axis. The two-point size evaluation is equivalent to the 2-

dimensional evaluation performed with all of the points projected onto any plane perpendicular to the cylinder axis.

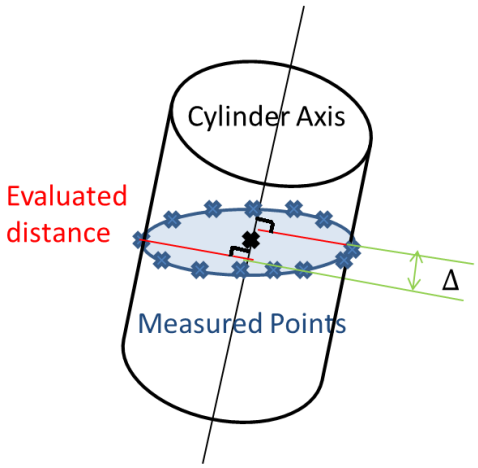

FIGURE 5.2: Misalignment of measurement and evaluation plane

5.2. Algorithms for Two-point Size

The key issue is to find the opposite point of each measurement point, and then the two-point size at each point could be obtained by adding up the distance of each point to the origin.

Each sampled point is offered with its (x_i, y_i, z_i) data, and could be transformed to (θ_i, r_i, z_i) information. The procedure of two-point size calculation for one arbitrary point is shown in FIGURE 5.3.

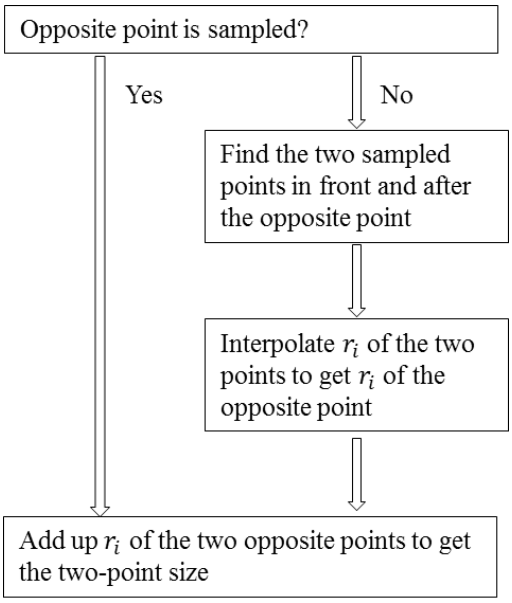

FIGURE 5.3: Procedure of calculation for two-point size

The opposite point of an arbitrary sampled point is 180 degree away from it through the center. It might be in the sampled points, then two-point size is calculated by adding up the radial distance of these two points. Most likely the opposite point is not sampled, then it is found by interpolating the two closest sampled points to it. The two points to be interpolated are the one in front of and the one behind the 180 degree point, and the result is the radial distance of the opposite point. The r_i of each point takes up its share weighted by how far it is to the opposite point in terms of center angle in the interpolation. The sampled points are taken every certain length of scanning, which means if the feature consists of arcs of different radii of curvature, the points are not evenly distributed by center angles. Therefore, to make sure the opposite point is in between the two searched points, we could not simply search for the two closest points to the opposite point. The two closest points might be on the same side of the opposite point, so the relative positions of the two points also matter.

These two points to be interpolated, denoted by the former point and latter point with respect to the opposite point, are searched separately in the sampled points, with three situations they might fall in.

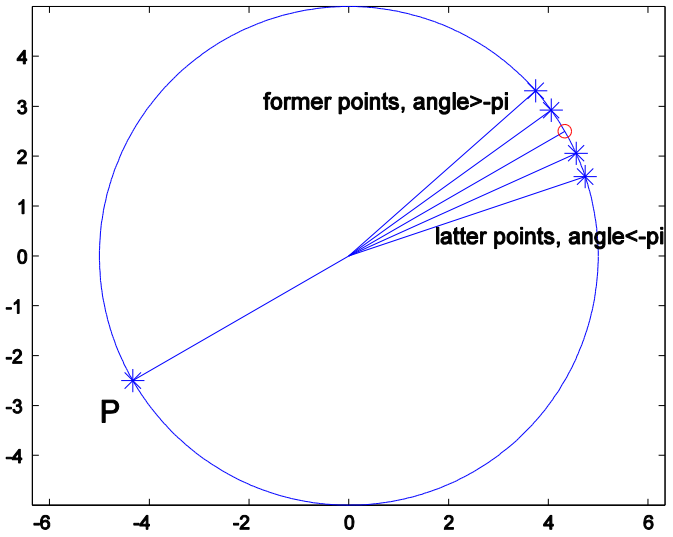

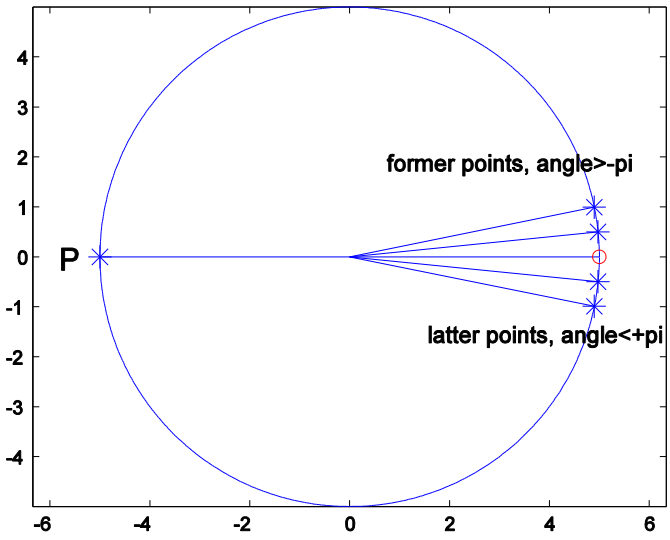

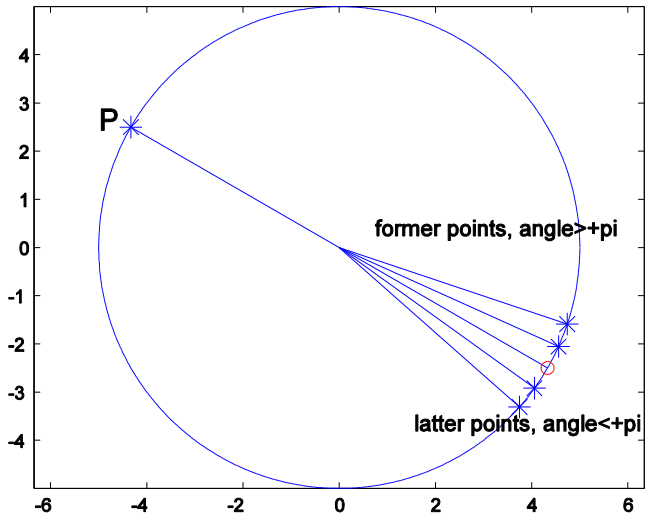

FIGURE 5.4: Three conditions when searching for interpolation points

FIGURE 5.4 is offered with a cylinder as an example, and is given under the condition that the points are collected clockwise. For counter clockwise points, just exchange the description 'former' with 'latter', which will not affect the result of the search.

When searching for the interpolating points for the opposite point of an arbitrary point P, the angles in FIGURE 5.4 refers to the difference of the center angles between the checked point and point P, and each sampled point is checked to find the adjacent points.

$$\Delta\theta_P = \theta_i - \theta_P \qquad (5.1)$$

The former point would be found when

$$\Delta\theta_P > \pi \;\&\; (\Delta\theta_P - \pi) \to \min, \text{if } \theta_P \in [0, \pi)$$

$$OR\ \Delta\theta_P > -\pi \;\&\; \big(\Delta\theta_P - (-\pi)\big) \to \min, \text{if } \theta_P \in [\pi, 2\pi) \qquad (5.2)$$

The latter point would be found when

$$\Delta\theta_P < \pi \;\&\; (\Delta\theta_P - \pi) \to \max, \text{if } \theta_P \in [0, \pi]$$

$$OR\ \Delta\theta_P < -\pi\ \&\ \left(\Delta\theta_P - (-\pi)\right) \to \max, \text{if}\ \theta_P \in (\pi, 2\pi) \qquad (5.3)$$

After the former and latter point are found, their information (θ_f, r_f) and (θ_l, r_l) could be used in the interpolation. Distance of the opposite point to the origin

$$r_{op} = r_f * \frac{\theta_f}{\theta_l - \theta_f} + r_l * \frac{\theta_l}{\theta_l - \theta_f} \qquad (5.4)$$

The two-point size at point P is

$$d_P = r_P + r_{op} \qquad (5.5)$$

For each sampled point, such a two-point size could be calculated.

5.3. Application to Data

5.3.1. Two-point Diameter of Cylinder

Firstly, two-point diameter of Part CYL_S2 was calculated and shown in FIGURE 5.5. If the two-point diameter of this cylinder is limited in a tolerance, for example 100.0 ± 0.15 mm, then all the measured points would be within tolerance. If, however, the tolerance is 100.0 ± 0.1 mm, there will be 8 points out of tolerance, and the part would be failed.

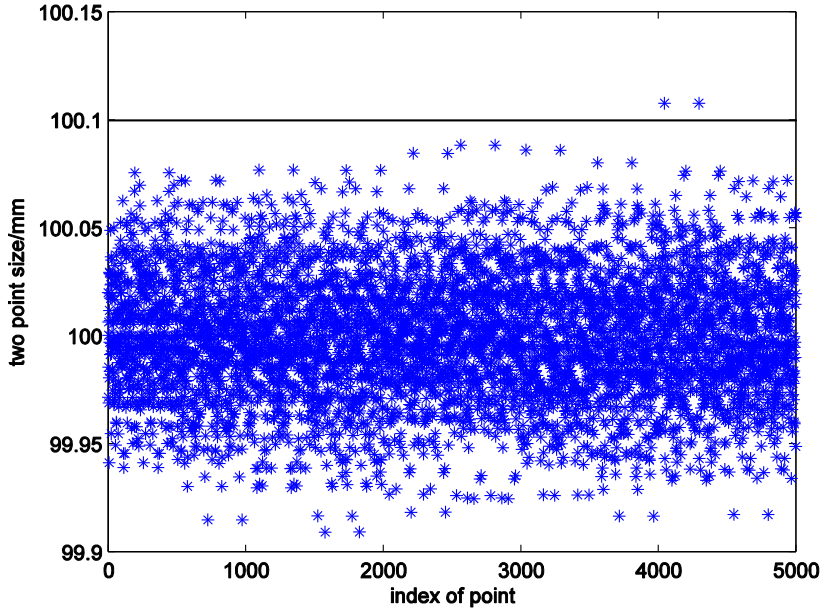

FIGURE 5.5: Two-point diameter at multiple points of the simulated cylinder

The two-point size could also be used together with other specification modifiers. For example, a restricted portion of the feature could be toleranced. If only the first 5 levels of the simulated cylinder is toleranced, which is point number 1 to 2500, the part will still be in tolerance if the tolerance is 100.0 ± 0.1 mm. Additionally, two-point size is one of the most used bases in calculation of rank-order size, which will be discussed in Chapter 6.

The two-point size of Part A was calculated as shown in FIGURE 5.6. As discussed in 4.2.1, there is a periodic pattern in the result because of the deviation from a circular shape of the part. The 20 peaks in the figure correspond to the two-lobe nature of the parts in 10 levels. The amplitude of the varying local sizes is approximately 8.4 μm according to the first period. The range of this period is 14.6 μm.

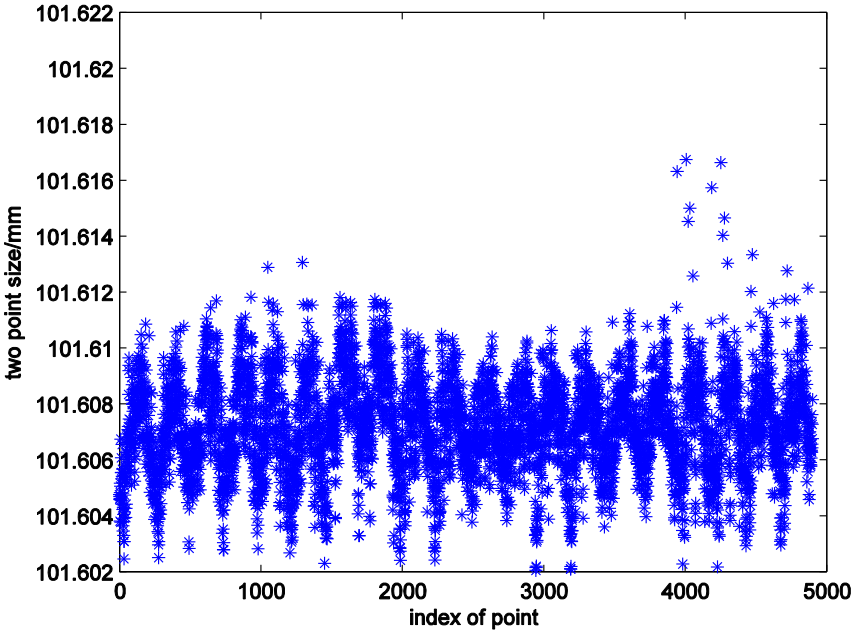

FIGURE 5.6: Two-point diameter at multiple locations of part A

Two-point size of Part B is calculated as shown in FIGURE 5.7. The amplitude of size variation of two-point diameters of Part B is slightly smaller than that of Part A, approximately 3.7μm for the first period. The dispersion is larger, range being 24.2 μm. This is also indicated in FIGURE 4.9 that the deviation from circular shape of part B is smaller than Part A, but there are more "spikes" in the form.

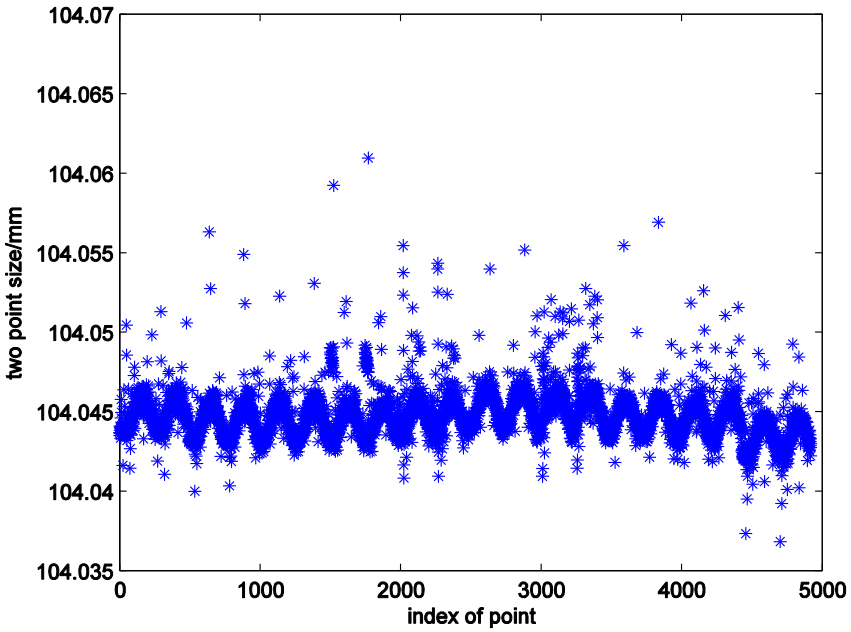

FIGURE 5.7: Two-point diameter at multiple locations of part B

5.3.2. Two-point Size of Constant Width Part

The two-point size of a constant width part should show a periodic change due to the characteristic of the shape. The two-point size is supposed to change smoothly and periodically, as shown in FIGURE 5.8. The two-point size reaches a peak when the line connecting the two points goes through one of the three centers of the arcs. It reaches a valley when that line is parallel to one of the three sides of the equilateral triangle formed

by the centers of the arcs. FIGURE 5.9 is a set of two-point size of one cross section of a Part CWP_S1, which is a perfect part with no deviation.

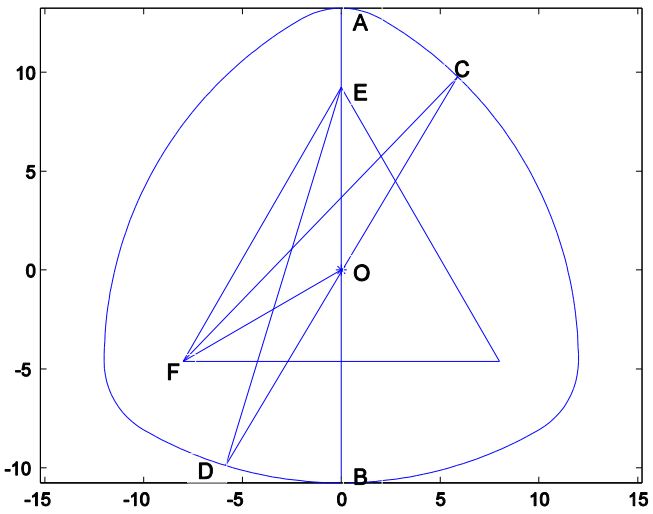

FIGURE 5.8: Peak and valley value of the two-point size of a constant width shape

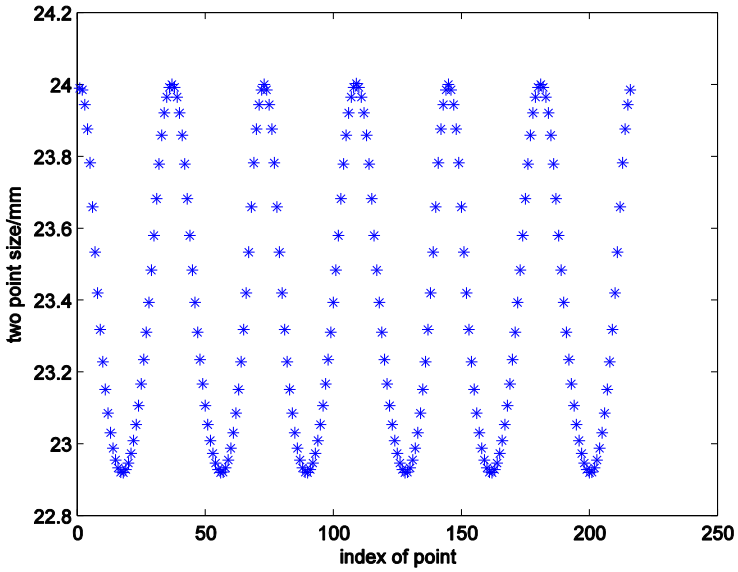

FIGURE 5.9: Two-point size at multiple points of one level of Part CWP_S1

One peak value is reached when the two points are at A and B in FIGURE 5.6. This size is a+2b=24. (a=16, b=4 for Part CWP_S1)

A valley value is reached when the two points are at C and D and CD//EF.

$$\angle \mathrm{FOC} = \frac{5\pi}{6}, FO = \frac{\sqrt{3}}{3}\mathrm{a}, \mathrm{FC} = \mathrm{R} = \mathrm{a} + \mathrm{b};$$

In $\Delta \mathrm{FOC}, FC^2 = FO^2 + OC^2 - 2 * FO * OC * \cos \angle FOC$

$$(a+b)^2 = \left(\frac{\sqrt{3}}{3}a\right)^2 + OC^2 - 2 * \left(\frac{\sqrt{3}}{3}a\right) * OC * \cos\left(\frac{5\pi}{6}\right)$$

Same in $\Delta \mathrm{EOD}$

$$(20)^2 = \left(\frac{\sqrt{3}}{3} * 16\right)^2 + OC^2 - 2 * \left(\frac{\sqrt{3}}{3} * 16\right) * OC * \cos\left(\frac{5\pi}{6}\right)$$

$$\mathrm{OC} = 11.4594$$

Therefore the valley value is 22.9188.

Two-point size of Part CWP_S2 was calculated, the center and axis being the least-squares fitted ones with the best convergence. The curve is not as smooth as that of Part CWP_S1 because of the form deviations added.

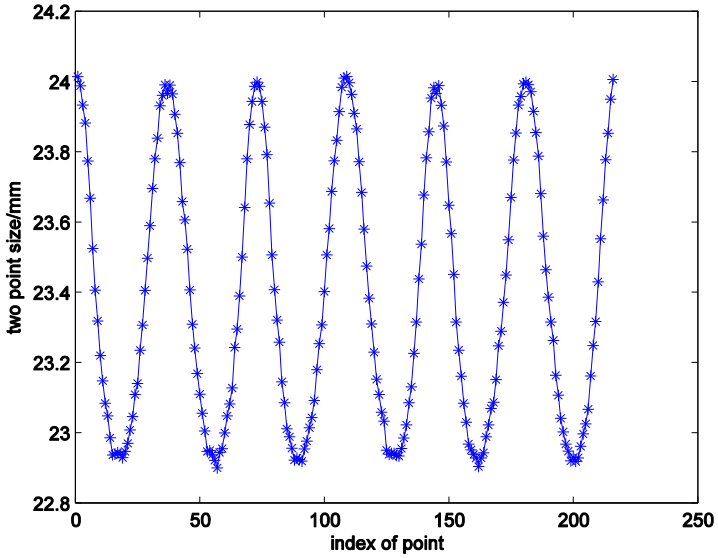

FIGURE 5.10: Two-point size at multiple points of one level of Part CWP_S1

Two-point size of measured Part C was calculated, result plotted in FIGURE 5.11. The variations of peak and valley values of the curve are partially due to the form of the actual part, and the uncertainty in the least-squares fitting since nominal parameters are not available. A more significant contributor is the defect on the part shown in FIGURE 5.12, which causes the second valley and the third peak of the curve to deviate.

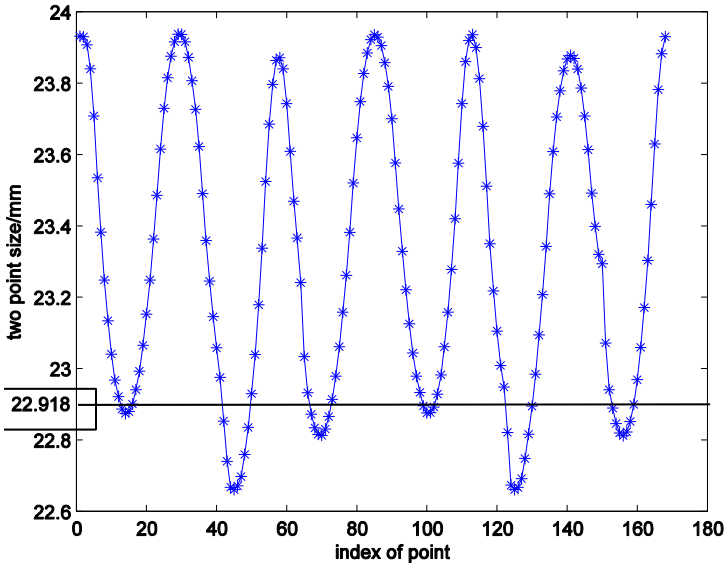

FIGURE 5.11: Two-point size at multiple points of one level of Part C

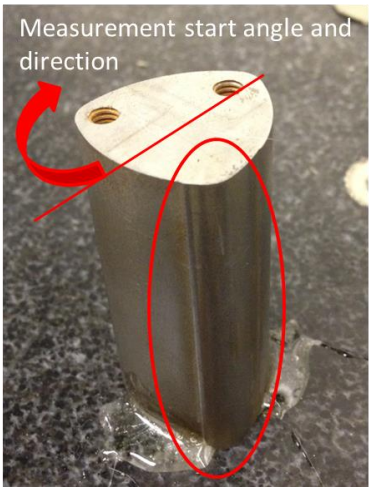

FIGURE 5.12: Defect on Part C

CHAPTER 6: RANK-ORDER SIZE

6.1. Introduction into Rank-order Size

Rank-order size is defined "mathematically from a homogeneous set of local size values contained along and/or around the tolerance feature" in ISO 14405-1 [5]. It is a statistical size to be used upon a set of local size values, which could be "portion size, section size, spherical size, and two-point size" [5]. Two-point size is the most commonly used local size together with any of the rank-order size. Rank-order size in ISO 14405-1 includes maximum size, minimum size, average size, median size, mid-range size and range of sizes.

6.2. Algorithms of Rank-order Size

Suppose a set of local size values be $\mathrm{D} = \{d_i\}, i = 1,2,3, \dots, n$. n is the total number of local size values collected or calculated.

6.2.1. Maximum Size (SX)

Maximum size is defined as "the maximum of the set of values of a local size along and/or around the tolerance feature".

6.2.2. Minimum Size (SN)

Minimum size is defined as "the minimum of the set of values of a local size along and/or around the tolerance feature".

6.2.3. Average Size (SA)

Average size is defined as “the average of the set of values of a local size along and/or around the tolerance feature”.

$$d_{avg} = \frac{1}{n}\sum_{i=1}^{n} d_i$$

6.2.4. Median Size (SM)

Median size is defined as “the median value of the set of values of a local size along and/or around the tolerance feature”. Given the arranged local size values from d_{min} to d_{max} in order, the median of the series $\{d'_1 = d_{min}, d'_2, d'_3, \dots, d'_{n-1}, d'_n = d_{max}\}$ is given by

$$d_{med} = \begin{cases} d'_{\frac{n+1}{2}}, & if\ n\ is\ odd \\ \dfrac{d'_{\frac{n}{2}} + d'_{\frac{n}{2}+1}}{2}, & if\ n\ is\ even \end{cases}$$

6.2.5. Mid-range Size (SD)

Mid-range size is defined as “the mean of the maximum and the minimum of the set of values of a local size along and/or around the tolerance feature”.

$$d_{mid} = \frac{d_{max} + d_{min}}{2}$$

6.2.6. Range of Sizes (SR)

Range of sizes is defined as “the difference between the maximum and the minimum of the set of values of a local size along and/or around the tolerance feature”.

$$d_{rng} = d_{max} - d_{min}$$

6.3. Application to Data

All calculations following are based on the two-point sizes at all points calculated in Chapter 5. For the cylinder, the result is the two-point diameter specifically. The rank-order sizes for simulated and measured parts are listed in Table 6.1.

TABLE 6.1: Rank-order sizes of example parts (mm)

Modifier	Description	Part CYL_S2	Part A	Part B	Part CWP_S2	Part C
SX	Maximum size	100.1076	101.6167	104.0610	24.0314	23.9575
SN	Minimum size	99.9091	101.6021	104.0368	22.8822	22.6605
SA	Average size	99.9994	101.6072	104.0448	23.3917	23.3378
SM	Median size	99.9988	101.6072	104.0447	23.3157	23.3008
SD	Mid-range size	100.0083	101.6094	104.0489	23.4568	23.3090
SR	Range of sizes	0.1985	0.0147	0.0241	1.1492	1.2970

FIGURE 6.1 and 6.2 show histograms of the two-point sizes of Part A and C respectively, with the marked rank-order sizes to display their positions among the population of samples.

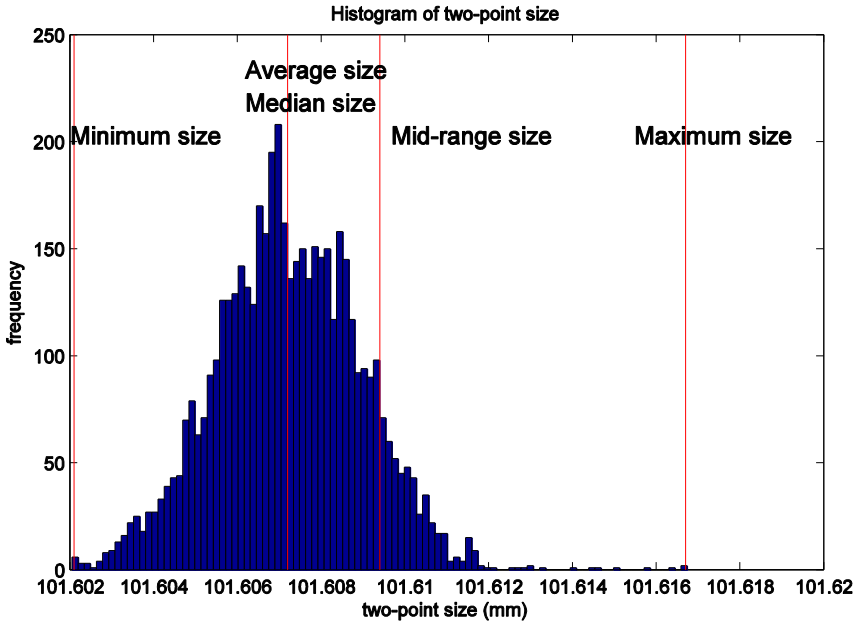

FIGURE 6.1: Two-point diameters of part A with rank-order sizes

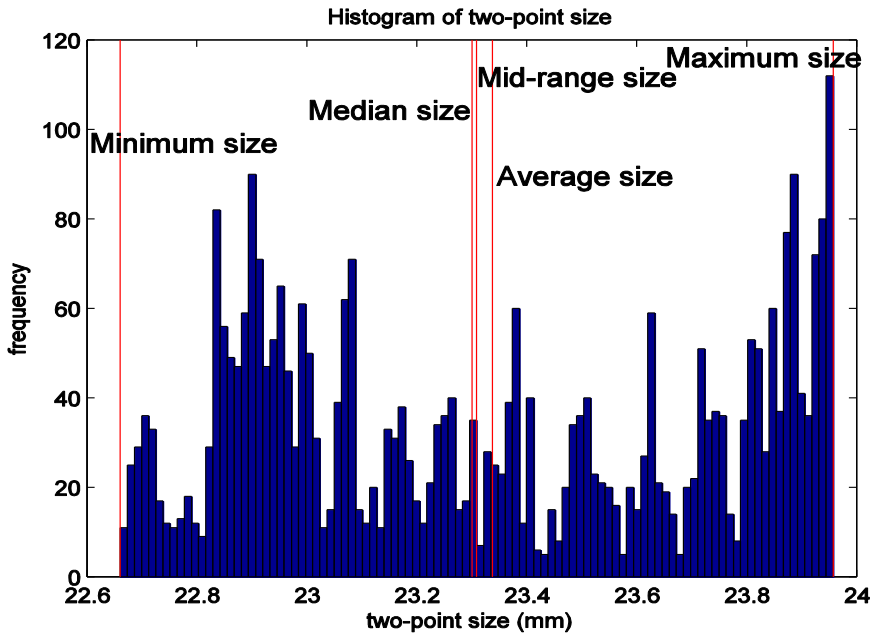

FIGURE 6.2: Two-point size of part C with rank-order sizes

6.4. Influence of Sampling Strategy

The same subsampling strategy same as in 4.3.2 is used to obtain the subsets of data with different data density. Each rank-order size of Part A for each subset of data is calculated, and their distribution displayed in FIGURE 6.3 through 6.8.

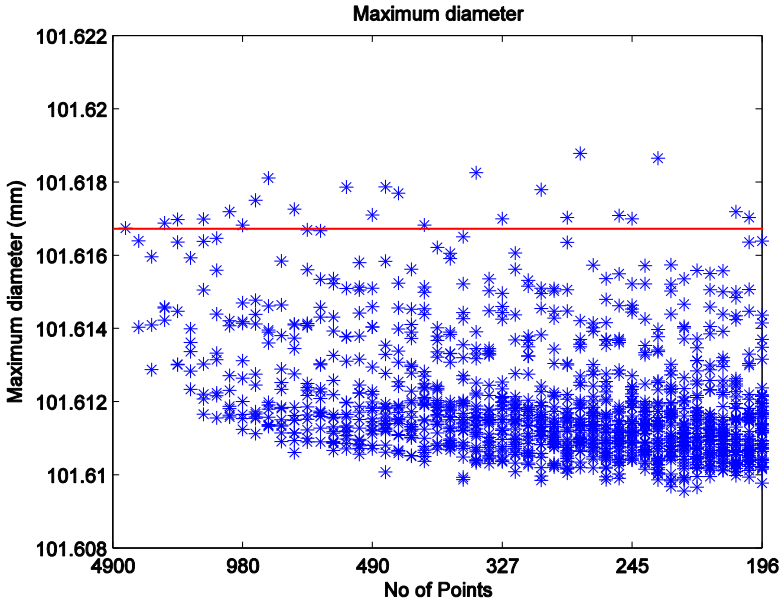

FIGURE 6.3: Maximum diameter for each subset

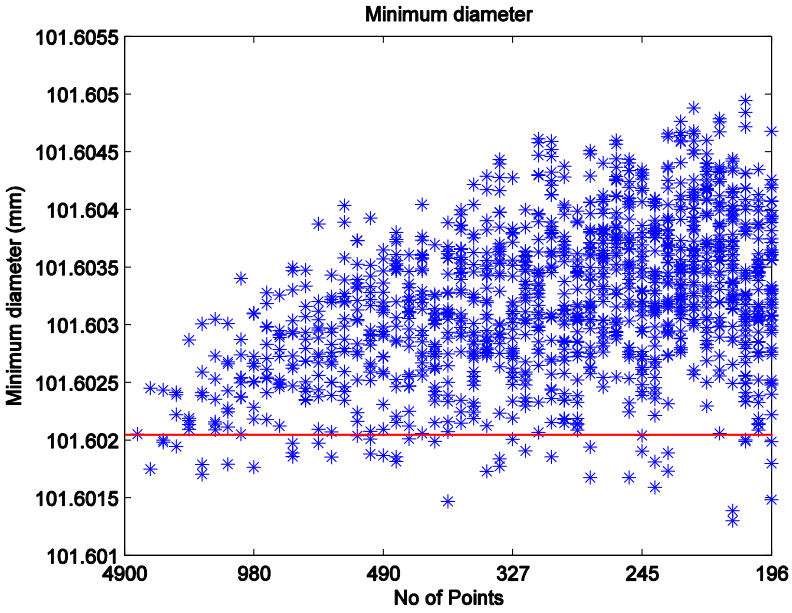

FIGURE 6.4: Minimum diameter for each subset

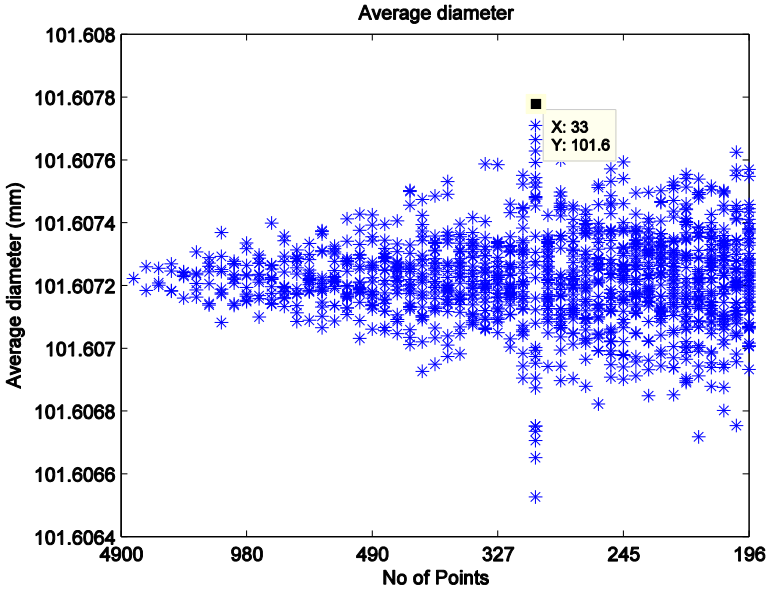

FIGURE 6.5: Average diameter for each subset

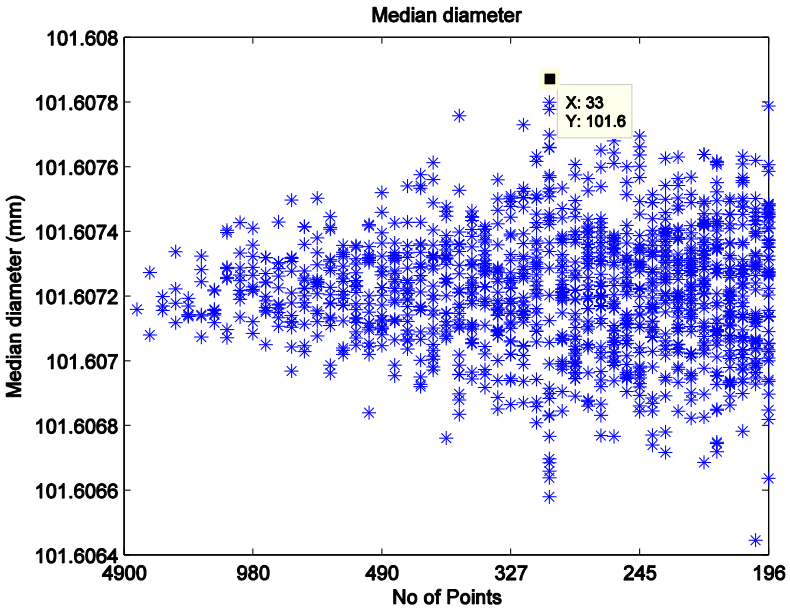

FIGURE 6.6: Median diameter for each subset

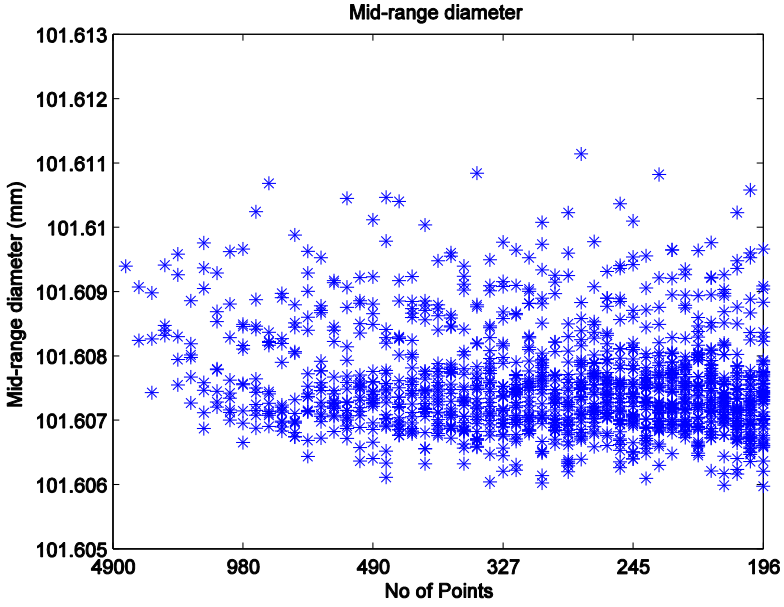

FIGURE 6.7: Mid-range diameter for each subset

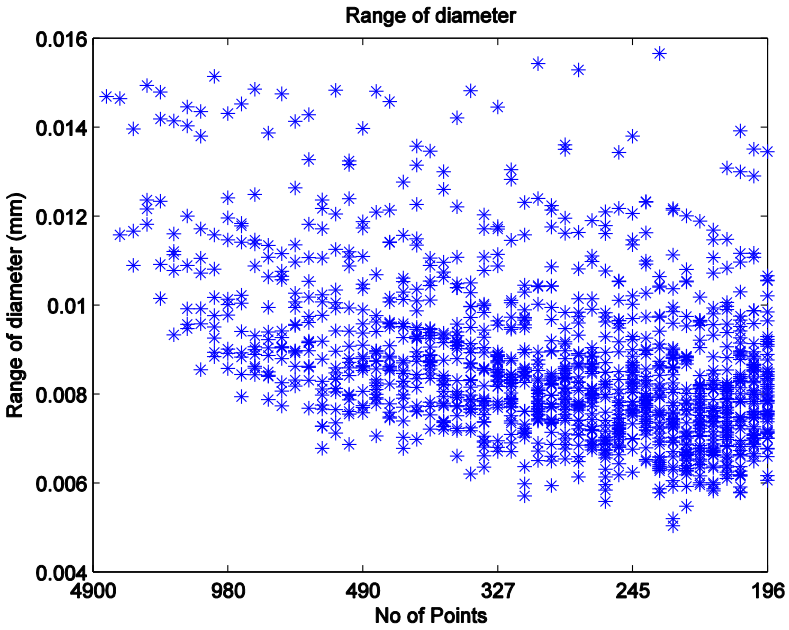

FIGURE 6.8: Range of diameter for each subset

Firstly, the dispersion of rank-order size increases with less sampling points, which indicates larger uncertainty in the calculation.

Secondly, for maximum diameter, this size of the first subset should be larger than that of any other subset. This is because the first group has the most sampling points, and should cover the largest diameter in all measurements. The subsets with less sampling points might lose this largest diameter during the sub sampling. Therefore, all the maximum size of the smaller samples should be smaller or equal to the maximum of the initial sample. However, in FIGURE 6.3, there are clearly larger diameters reached in the smaller sample groups. This is due to the interpolation method used to calculate the two-point size. As in FIGURE 6.9, different points are used in the interpolation in samples of different sampling frequency. Therefore, it is possible that the interpolation result of points in a smaller sampling frequency group is larger than that of points in larger sampling frequency.

This interpolation issue could be more clearly shown by an example of the constant width part measured with 3 points. If the three sampled points are at the positions as in FIGURE 6.10, the interpolation of the opposite point would be between the other two maxima, marked by the square. However the actual opposite point should be the circled point.

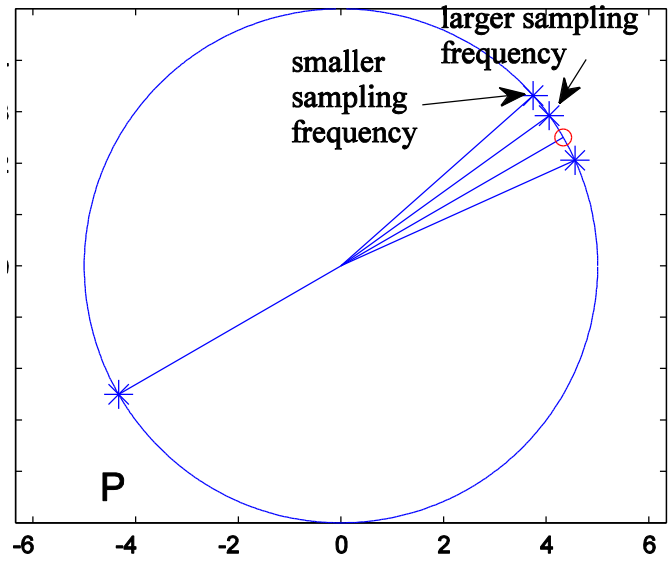

FIGURE 6.9: Interpolation points of different sampling frequency

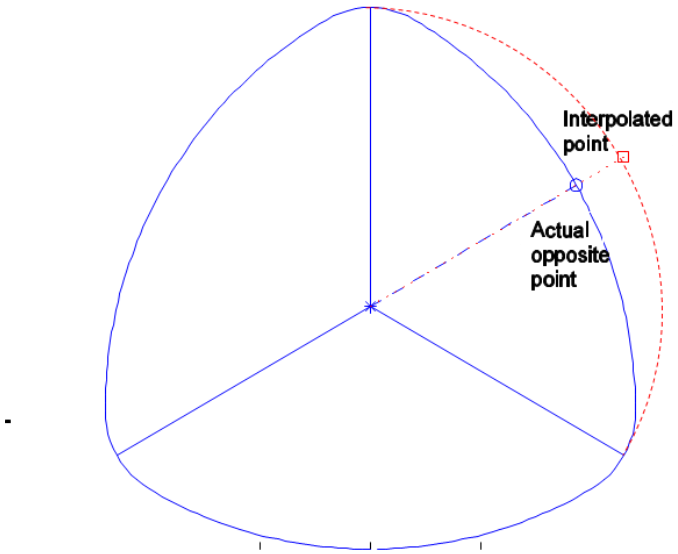

FIGURE 6.10: Interpolation of selected points on a constant width part

Finally, in FIGURE 6.5 and 6.6, similar with the findings about FIGURE 4.13, dispersion of the sizes of group no 33, the subsets in which contain 148 or 149 points, is much larger than the other groups. This is also due to the interaction with manufacturing process.

\

CHAPTER 7: CONCLUSIONS AND FUTURE WORK

7.1. Conclusions

This thesis reviewed 8 of the 14 types of size defined in ISO 14405-1. Explicit algorithms were offered for calculation of each size. Characteristics of the sizes and their application with two example parts were discussed. The constant width part was included to address some characteristics of two-point size specifically. Some consideration of uncertainty was offered at the same time.

The least-squares size is sensitive to the initial guess, errors in the measured points, sampling strategy and certain characteristics of the part. For least-squares criterion, the initial guess is important because of the non-linear nature of the problem Especially for constant width part, the effect of initial guess is significant. The calculation time is much longer than cylinder due to the complexity of the shape definition and the method used. Uncertainty analysis under limited conditions was offered. The errors of each input point are averaged out in the fitting procedure. Sampling strategy introduces larger uncertainty in the result, especially when the sampling interacts with characteristics of the part surface.

For two-point size, the algorithms were offered. Two-point size is influenced by the shape of the part and possible defects on the actual part. Its deviation from the actual two-point size is due to the approximation of assessment cross-section, associated center, and due to the interpolation method. With coordinate information of multiple sampling

points, the key procedure is to identify the opposite points. A periodic pattern showed due to the deviation from the circular shape of the measured parts. Otherwise, the two-point size appeared to be approximately Gaussian distributed for the simulated part. Two-point size of constant width part should show smooth and stable periodic change. However, defect on the measured constant width part introduced a lot more variations.

For rank-order sizes, which are based on the two-point sizes, the algorithms for each rank-order size were offered. Rank-order sizes are sensitive to sampling strategy and characteristics of the part. Due to the interpolation method used in calculation of two-point size, the data sets with smaller sampling density might result in larger maximum/smaller minimum sizes than those with larger sampling density.

A journal paper was published as a summary of the initial work [23].

7.2. Future Work

This thesis offered some insights into understanding and application of size specifications in the ISO standard. The uncertainty analyses were merely a simple investigation into the influences, which could be improved by carrying out task specific uncertainty analyses. Besides, 6 more sizes are to be investigated as extended work. Experiences of investigating them could be implemented into analysis of the rest of the size definitions.

In addition to the application of the size definitions to simple features, another important aspect is to explore their application in industry. For what design purposes would these sizes be significant, what are the dominant features then, and how the GD&T would be specified with these sizes, are some important questions to be answered.

BIBLIOGRAPHY

[1] Morse, E. P., Srinviasan, V., "Size Tolerancing Revisited: A Basic Notion and Its Evolution in tandards," *Proceedings of the Institution of Mechanical Engineers, Part B: Journal of Engineering Manufacture,* pp. 227(5) 662-671, 2013.

[2] E. P. Morse, "Advanced Coordinate Metrology Lecture Notes," UNC Charlotte, Charlotte, 2013.

[3] *ISO 14638:2015 Geometrical product specifications (GPS) -- Matrix model,* Geneva: ISO, 2015.

[4] *ASME Y14.5-2009, Dimensioning and Tolerancing,* New York: The American Society of Mechanical Engineers, 2009.

[5] *ISO 14405-1: 2010 Geometrical Product Specifications (GPS) - Dimensional Tolerancing - Part 1: Linear Sizes,* Geneva: ISO, 2010.

[6] H. Voelcker, "Let's talk about size," *mfg magazine,* vol. 2, no. 1, 1995.

[7] H. Voelcker, "'Size' revisited," *mfg magazine,* vol. 8, no. 1, 2001.

[8] H. Voelcker, "Whither 'Size' in Geometric Tolerancing," *Proc. ASPE Summer Topical Meeting onTolerance Modeling and Analysis,* 2002.

[9] *ISO 5459:2011 Geometrical Product Specifications (GPS) - Dimensional Tolerancing - Datums and Datum Systems,* Geneva: ISO, 2011.

[10] ISO, *14405-2:2011 Geometrical product specifications (GPS) - Dimensional tolerancing - Part 2: Dimensions other than linear sizes,* Geneva: ISO, 2011.

[11] Srinivasan, V., Shakarji, G. M., Morse, E. P., "On the Enduring Appeal of Least-Squares Fitting in Computational Coordinate Metrology," *Computing and Information Science in Engineering,* vol. 12, pp. 011008-1, 2012.

[12] Per Christian Hansen, V ́ctor Pereyra, Godela Scherer, Least Squares Data Fitting with Applications, Baltimore: The Johns Hopkins University Press, 2012.

[13] Lagarias, J.C., Reeds, J.A., Wright, M.H., Wright, P.E., "Convergence Properties of The Nelder-Mead Simplex Method in Low Dimensions," *SIAM Journal of Optimization,* vol. 9, no. No. 1, pp. 112-147, 1998.

[14] C. M. Shakarji, "Least-squares fitting algorithms of the NIST alogrithm testing system," *Journal of Research of the National Institute of Standards and Technology,*

vol. 103, no. 6, pp. 633-641, 1998.

[15] A. B. Forbes, "Least-squares best-fit geometric elements," NPL, Teddington, 1991.

[16] *Prismo Specifications.* [Performance]. Zeiss, May 2013.

[17] M. S. Shunmugam, "On assessment of geometric errors," *INT. J. PROD. RES.*, vol. 24, no. 2, pp. 413-425, 1986.

[18] J. Bonnans, Numerical Optimization: Theoretical and Practical Aspects, Berlin, New York: Springer, 2006.

[19] BIPM, "Evaluation of Measurement Data - Supplement 1 to the "Guide to The Expression of Uncertainty in Measurement" - Propagation of Distributions Using a Monte Carlo Method," 2008.

[20] ISO, "10360-4 Geometrical Product Specifications (GPS) -- Acceptance and Reverification Tests for Coordinate Measuring Machines (CMM) -- Part 4: CMMs Used in Scanning Measuring Mode," 2000.

[21] BIPM, "Evaluation of Measurement Data - Suppliment 2 to the "Guide to The Expression of Uncertainty in Measurement" - Extension to any Number of Output Quantities," 2011.

[22] *ISO 14660-2: Geometrical Product Specifications (GPS) - Geometrical Features - Part 2: Extracted Median Line of a Cylinder and a Cone, Extracted Median Surface, Local Size of an Extracted Feature*, Geneva: ISO, 1999.

[23] Edward Morse, Yue Peng, Vijay Srinivasan, Craig Shakarji, "Metrological challenges introduced by new tolerancing standards," *Meas. Sci. Technol.* , vol. 25, 2014.